catalysts

MDPI

Article

Photochemical Study of a New Bimolecular Photoinitiating System for Vat Photopolymerization 3D Printing Techniques under Visible Light

Paweł Fiedor [1], Maciej Pilch [1], Patryk Szymaszek [2], Anna Chachaj-Brekiesz [2], Mariusz Galek [3] and Joanna Ortyl [1,3,*]

[1] Faculty of Chemical Engineering and Technology, Cracow University of Technology, Warszawska 24, 31-155 Cracow, Poland; pawfie68@gmail.com (P.F.); pilchmac@gmail.com (M.P.)
[2] Faculty of Chemistry, Jagiellonian University, Gronostajowa 2, 30-387 Cracow, Poland; szymaszek.patryk@gmail.com (P.S.); chachaj@chemia.uj.edu.pl (A.C.-B.)
[3] Photo HiTech Ltd., Bobrzyńskiego 14, 30-348 Cracow, Poland; mariusz.galek@photohitech.com
* Correspondence: jortyl@chemia.pk.edu.pl

Received: 10 January 2020; Accepted: 14 February 2020; Published: 2 March 2020

Abstract: In this work, we presented a new bimolecular photoinitiating system based on 2-amino-4,6-diphenylpyridine-3-carbonitrile derivatives as visible photosensitizers of diphenyliodonium salt. Real-time FTIR and photo-DSC photopolymerization experiments with a cycloaliphatic epoxide and vinyl monomers showed surprisingly good reactivity of the bimolecular photoinitiating systems under UV-A, as well as under visible light sources. Steady-state photolysis, fluorescence experiments, theoretical calculations of molecular orbitals, and electrochemical analysis demonstrated photo-redox behavior as well as the ability to form initiating species via photo-reduction or photo-oxidation pathways, respectively. Therefore, the 2-amino-4,6-diphenylpyridine-3-carbonitrile derivatives were also investigated as a type II free-radical photoinitiator with amine. It was confirmed that the 2-amino-4,6-diphenylpyridine-3-carbonitrile derivatives, in combination with different types of additives, e.g., amine as a co-initiator or the presence of onium salt, can act as bimolecular photoinitiating systems for cationic, free-radical, and thiol-ene photopolymerization processes by hydrogen abstraction and/or electron transfer reactions stimulated by either near-UV or visible light irradiation. Finally, the 2-amino-4,6-diphenylpyridine-3-carbonitrile derivatives were selected for 3D printing rapid prototyping experiments. Test objects were successfully printed using purely cationic photosensitive resin, created on a 3D printer with a visible LED light source.

Keywords: photopolymerization; photo-redox initiating system; 3D printing; additive manufacturing; digital light processing; stereolithography; photosensitizers; photo-reduction; photo-oxidation

1. Introduction

Three-dimensional printing is a technique used for the quick fabrication of three-dimensional objects based on virtual CAD documentation. This process enables a 3D printer to print an object in three-dimensions in a layer-by-layer manner. Therefore, the essence of the rapid prototyping (RP) is that it shapes the work piece not by removing material, as is the case with machining processes, but by adding material [1]. The additive manufacturing (AM) process allows the creation of complex geometries that cannot be obtained by machining. Moreover, the AM method allows for a shortened process of preparation and execution of the model, i.e., the prototype of the final product or its components. It also facilitates the modification of the shape and sometimes the product properties in

the early stages of development. There are several technologies for creating models. Their common feature is that the object is built in layers, but due to the cost of equipment and consumables on a large scale only a few rapid prototyping systems are used, such as stereolithography (SLA) [2], digital light processing (DLP) [3,4], continuous liquid interface production (CLIP) [5], layered application and curing of photopolymers (PolyJet) [6], fused deposition liquid plastic modelling (FDM) [7], selective laser sintering (SLS) [8], and selective laser melting (SLM) [9].

The development of digital technologies and the design of 3D printers made it possible to obtain high print resolutions, and the main limitation was the photocurable material itself [10]. In order to develop 3D printing technologies further, it became necessary to create new photosensitive compositions and appropriate initiating systems. Most commercial photosensitive resins for 3D printing applications are based on a free-radical type of photocurable acrylate resin [11]. In addition to traditional radical polymerization, reports can be found in the literature on the use of cationic polymerization [12]. This approach resulted in the elimination of the negative effect of oxygen on free-radical polymerization [13]. Cationic photoinitiators, however, suffer from insufficient activity and speed of polymerization in 3D printing processes in new machines, which use visible LED light sources [14] with maximum emission of 405 or 450 nm. A solution to this problem may be the introduction of a bimolecular initiating system into the photocurable material [15]. Bimolecular initiating systems consist of two independent constituents, an onium salt photoinitiator and a light absorbing photosensitizer [16,17]. By matching spectra of curing light with absorption spectra of photosensitizers, bimolecular photoinitiating systems allow the more efficient use of light in the photopolymerization initiation process [18]. Another advantage of bimolecular systems is the limitation of the depth of light penetration in the photosensitive resin by controlling the concentration of the photosensitizer, which results in high resolution prints [19]. At the design stage of a two-component initiating system, many factors should be taken into account, including the absorption spectrum of the tested compound and its photostability. Strong photogenerated protic acids, formed during the initiation of photopolymerization in a bimolecular system, can cause degradation of the photosensitizer. The most desirable effect of degradation is photobleaching of the polymeric material; however, this effect is rarely observed. If a fluorescent molecule is used as a photosensitizer in a bi-component initiating system, it can be utilized to track changes occurring in the environment during the photopolymerization process [20]. Such molecules are called fluorescent molecular sensors and can be used to measure the kinetics of the process; upon validation, they indirectly determine the conversion of the polymerizing formulation. The technique of investigating polymerization parameters by analyzing changes in fluorescent spectra is called Fluorescent Probes Technique (FPT) [21–25]. Although both onium salt photosensitizers and fluorescent molecular sensors for photopolymerization processes have been extensively described, their combination into a two-component photoinitiating system [26] for purely photosensitive cationic resin for 3D printing application is rather unique [27–29].

A recent report studied 2-amino-4,6-diphenylpyridine-3-carbonitrile derivatives as fluorescent molecular probes for monitoring the cationic photopolymerization of monomers using the Fluorescence Probe Technique (FPT). It was found that the 2-amino-4,6-diphenylpyridine-3-carbonitrile derivatives accelerate cationic photopolymerization initiated with diphenyliodonium photoinitiators at the wavelength where the photoinitiator alone does not work [30]. It was revealed that these compounds accelerate the cationic photopolymerization process and serve as probes for monitoring the polymerization progress at the same time. It was shown that the sensitization efficiency of the 2-amino-4,6-diphenylpyridine-3-carbonitrile derivative probes depends on the type of substituent on the pyridine moiety. As pointed out by Crivello [31], the effectiveness of photosensitization of diphenyliodonium photoinitiators depends on the magnitude of Gibbs energy change for the electron transfer (ΔG_{ET}). A sensitizer is effective only when (ΔG_{ET}) is negative. The free enthalpy (ΔG_{ET}) is related to the oxidation and reduction of the reacting species and energy of the excited state by the equation originally proposed by Rehm and Weller [32], where the excited 2-amino-4,6-diphenylpyridine-3-carbonitrile molecule plays the role of donor (D),

diphenyliodonium photoinitiator is the acceptor (A) and the monomer is the solvent. Therefore, the use of photosensitizers with electron-donor substituents decreases the oxidation potential of sensitizers, which results in less negative values (ΔG_{ET}). For this purpose, we proposed in this paper the use of novel 2-amino-4,6-diphenylpyridine-3-carbonitrile derivatives with an electron-donating group incorporated into this structure moiety that will further increase the efficiency of sensitization. The new compounds with better spectroscopic properties and lower oxidation potentials were examined as components of visible light photoinitiating systems for different types of photopolymerization processes. These 2-amino-4,6-diphenylpyridine-3-carbonitrile derivatives were incorporated into two-component photoinitiating systems (PISs) to generate reactive species (radicals or cations) in order to initiate both the free radical polymerization of (meth)acrylates and the cationic polymerization of epoxides and vinyl ether monomers upon near-UV or visible light (LED at 365 nm, LED at 405 nm). Moreover, the chemical mechanisms were investigated through the analysis of their absorption properties, steady state photolysis, molecular orbitals, excited state processes and production of radicals.

2. Results and Discussion

2.1. Light Absorption and Fluorescence Properties of the 2-Amino-4,6-Diphenyl-Pyridine-3-Carbonitrile Derivatives

The 2-amino-4,6-diphenyl-pyridine-3-carbonitrile derivatives (S1–S8) were synthesized by a modified procedure described previously in the literature. The structure and purity of obtained products were confirmed by ^{1}H NMR, ^{13}C NMR and LC–MS analyses (see Supplementary Materials). Firstly, the absorption characteristics of the synthesized 2-amino-4,6-diphenyl-pyridine-3-carbonitrile derivatives were investigated in acetonitrile solutions (Figure 1). For efficient photoinitiation, the selection of a suitable photoinitiator is critical; therefore, it is necessary that the spectrum of the photoinitiator overlap with the emission spectrum of the light sources. As shown in Figure 1, derivatives of 2-amino-4,6-diphenyl-pyridine-3-carbonitrile exhibit maximum long-wavelength absorption in the range 349–365 nm, and peak extinction coefficients within 12,000–28,000 [dm^3·mol^{-1}·cm^{-1}]. Their maximum extinction coefficients and the corresponding wavelengths are reported in Table 1.

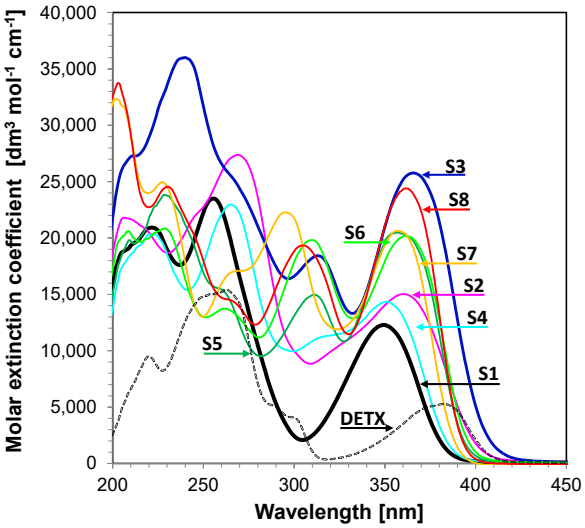

Figure 1. Ultraviolet (UV)–visible absorption spectra of the 2-amino-4,6-diphenyl-pyridine-3-carbonitrile derivatives and 2,4-diethyl-9*H*-thioxanthen-9-one (DETX) in acetonitrile.

The investigated compounds showed strong absorption at near UV and visible light regions, making them suitable for irradiation by LED sources with maximum emission at 365 and 405 nm. Thanks to the high extinction coefficient at 365 nm and minor extinction coefficient at 405 nm, those compounds are great candidates as both photosensitive components of photoinitiating systems and light depth penetration modulators. Light penetration depth is an important factor due to the application of such compounds into photocurable compositions dedicated to 3D printing. Circumscription of light penetration elongates the lifetime of photocurable resin, and prevents unwanted initiation of the polymerization process by residual photons driving through the resin bath. This effect also enhances the resolution of prints by limiting the region of curing.

Table 1. Light absorption and fluorescence data of investigated compounds in acetonitrile: maximum absorption wavelengths ($\lambda_{Ab\text{-}max}$), molar extinction coefficients (ε) at $\lambda_{Ab\text{-}max}$, and, at the emission wavelengths of the LEDs, maximum emission wavelengths ($\lambda_{Fl\text{-}max}$), Stokes shift.

Abb.	$\lambda_{Ab\text{-}max}$ [nm]	ε@λ_{max} [$dm^3 \cdot mol^{-1} \cdot cm^{-1}$]	ε@365 nm [$dm^3 \cdot mol^{-1} \cdot cm^{-1}$]	ε@405 nm [$dm^3 \cdot mol^{-1} \cdot cm^{-1}$]	$\lambda_{Fl\text{-}max}$ (λ_{ex}= 320 nm)	Stokes Shift [nm]	Intensity @$\lambda_{Fl\text{-}max}$ [a. u.]
S1	349	12,290	8410	100	418	69	19,890
S2	360	15,030	14,730	950	497	137	9110
S3	365	25,770	25,770	2810	480	115	17,410
S4	351	14,360	11,090	150	414	63	97,390
S5	356	20,500	19,820	310	418	62	125,020
S6	361	20,170	19,980	470	420	59	115,380
S7	357	22,270	19,240	110	411	54	43,650
S8	362	24,390	24,000	120	410	48	49,150

The fluorescence spectra of 2-amino-4,6-diphenyl-pyridine-3-carbonitrile derivatives are presented in Figure 2 and the corresponding data are listed in Table 1. The pyridine derivatives containing different phenyl units were found to exhibit different fluorescence properties, but all emitted fluorescence at the blue–green region of light between 410 and 500 nm. The spectroscopic properties of investigated compounds are strongly dependent on their structure. The introduction of an electron donor group, such as -SCH3, gives compounds 2-amino-4-(4-methylthiophenyl)-6-phenylpyridine-3-carbonitrile (S4), 2-amino-4-phenyl-6-(4-methyl-thiophenyl)pyridine-3-carbonitrile (S5), and 2-amino-4,6-bis(4-methylthiophenyl)-pyridine-3-carbonitrile (S6). For these compounds, the extinction coefficient value was greatly improved compared to the S1 compound. The selected derivatives of 2-amino-4,6-diphenyl-pyridine-3-carbonitrile (S4, S5 and S6) demonstrate huge enhancement of fluorescence intensity. Further modification of compound S1, by introduction of both electron donor and electron acceptor moieties, gave 2-amino-4-(4-methylthiophenyl)-6-(4-cyanophenyl)-pyridine-3-carbonitrile (S2) and 2-amino-4-(4-cyanophenyl)-6-(4-methylthiophenyl)-pyridine-3-carbonitrile (S3). Both of these compounds showed significant red-shift of maximum emission wavelength with a simultaneous decrease of fluorescence intensity at maximum wavelength. Moreover, for compounds S7 and S8, with two electron donor moieties on both phenyl rings of the 2-amino-4,6-diphenyl-pyridine-3-carbonitrile chromophore, a twofold increase of the extinction coefficient and fluorescence intensity was observed.

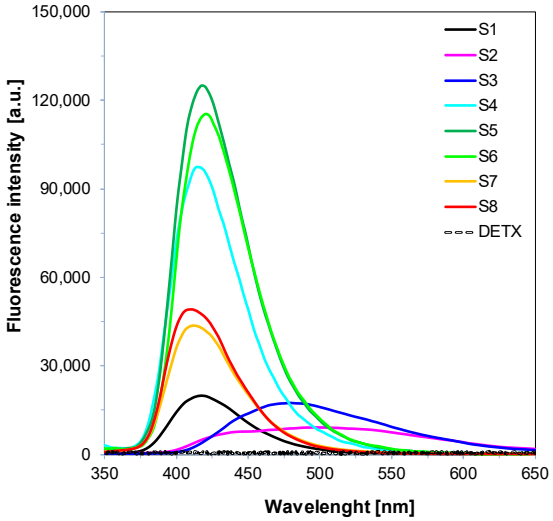

Figure 2. Fluorescence spectra of the 2-amino-4,6-diphenyl-pyridine-3-carbonitrile derivatives in acetonitrile in extinction at 320 nm with integration time of 1 s.

The results of computer simulations confirm the assumptions about the nature of the occupation of molecular orbitals in the analyzed molecules (all collected data are in the Supplementary Materials). In the unsubstituted molecule 2-amino-4,6-diphenylnicotinonitrile (S1), HOMO orbitals predominate in the part of the molecule where nucleophilic groups, such as amino groups and nitrogen in the aromatic ring, are located. The situation changes when the thiomethyl group is substituted on the other side of the molecule (structures S2,4). Then, the electron-occupied HOMO orbitals are located in the part of the molecule containing the thiomethyl group, due to the strong nucleophilic nature of this group. However, it can be suspected that the nucleophilic nature of thiomethyl and amino groups located in different parts of the molecule also partially cause more significant blurring of HOMO orbitals. The opposite situation is observed in the case of S3 and S5 molecules, where all nucleophilic moieties are located in one part of the molecule. In this case, the effects of nucleophilic groups strengthen each other, suggesting that these structures will be the most active in the electron transfer process. For the S6 molecule, containing thiomethyl groups symmetrically substituted on both sides, we observed the analogous HOMO orbitals system as in the unsubstituted structure S1. This indicates that the nucleophilic nature of these substituents is mutually suppressed. In the S7 and S8 structures, we observed the dispersion of HOMO orbitals caused by the presence of unequal nucleophilic moieties in both parts of the molecules (-SCH_3 and –OCH_3 group). Due to the potentially stronger nucleophilic nature of the thiomethyl group, in the S7 structure, electron-occupied HOMO orbitals occur in both parts of the molecule. Meanwhile, for the S8 molecule, HOMO orbitals are observed only in the part of the molecule with a stronger nucleophilic character.

2.2. The 2-Amino-4,6-Diphenyl-Pyridine-3-Carbonitrile Derivatives as Photosensitizers of Iodonium Salts: Investigation into the Photo-Induced Electron Transfer Process with the Photo-Oxidation Mechanism

Spectroscopic studies revealed that 2-amino-4,6-diphenyl-pyridine-3-carbonitrile derivatives could be applied as near UV and visible light photosensitizers of iodonium salts. This part of the paper describes the mechanical investigation and assessment of the photosensitization of 2-amino-4,6-diphenylpyridine-3-carbonitrile derivatives in combination with iodonium salt. It is well known that the main prerequisite for the photo-induced electron transfer (PET) process is that the thermodynamic driving force of the electron transfer reaction between the excited state of the photosensitizers and iodonium salt have a negative value. The free energy of activation for the PET (ΔG_{ET}) process can be easily estimated on the basis of the Rehm–Weller equation. The measured

oxidation potential of 2-amino-4,6-diphenyl-pyridine-3-carbonitrile derivatives and all calculated thermodynamic parameters are compiled in Table 2.

Table 2. Parameters characterising the photochemical reactivity of the 2-amino-4,6-diphenyl-pyridine-3-carbonitrile derivatives with diphenyliodonium hexafluorophosphate.

Abb.	$E_{ox}^{1/2}$ [mV]	$E_{00(S1)}$ [eV]	$E_{00(T1)}$ [eV]	$\Delta G_{ET(S1)}$ [eV]	$\Delta G_{ET(T1)}$ [eV]	K_{SV} [M^{-1}]	$\Phi_{ET(S1)}$
S1	1584	311	2.57	−0.92	−0.23	35.74	0.46
S2	1494	297	2.46	−0.86	−0.21	27.67	0.39
S3	1412	290	2.45	−0.87	−0.28	40.87	0.49
S4	1385	304	2.57	−1.04	−0.32	61.30	0.59
S5	1503	308	2.46	−0.97	−0.31	33.21	0.44
S6	1359	302	2.51	−0.72	−0.36	42.31	0.50
S7	1489	307	2.54	−0.98	−0.29	38.22	0.47
S8	1483	306	2.52	−0.97	−0.28	27.85	0.40

$E_{ox}^{1/2}$—electrochemically determined oxidation half-wave potentials (vs. Ag/AgCl) of the photosensitizers (the electron donor); $E_{00(S1)}$—excitation energy of the photosensitizer, which is referred to as singlet excitation energy; extracted from the UV-vis absorption and fluorescence emission spectra; $E_{00(T1)}$—triplet state energies were calculated on the basis of the uM06/6-31G level of theory, $\Delta G_{ET(S1)}$—enthalpy of free electron transfer from singlet state were calculated from the classical Rehm–Weller equation; the reduction half-wave potentials of the diphenyliodonium hexafluorophosphate (HIP) (the electron acceptor) $E_{red}^{1/2}{}_{HIP} = -0.68$ V vs. SCE (−0.72 V vs. Ag/AgCl) [33,34]; $\Delta G_{ET(T1)}$—enthalpy of free electron transfer from triplet state from the Rehm–Weller equation; $\Phi_{ETt(S1)}$ electron transfer quantum yields with diphenyliodonium hexafluorophosphate (the electron acceptor), with concentration [IOD]=2,1·10^{-2} mol·dm^{-3}.

Examples of cyclic voltammograms are included in the Supplementary Materials. The singlet excited state energy values necessary to calculate $\Delta G_{ET(S1)}$ were determined on the basis of the crossing of the excitation and emission spectra. Triplet excited state energies were estimated from molecular orbital calculations (uB3LYP/6-31G (d,p) level of theory). The calculations clearly show that all combinations of the 2-amino-4,6-diphenyl-pyridine-3-carbonitrile derivatives with iodonium salt possess a high driving force upon exposure to light. This means that for the tested photo-redox pairs, the photo-induced intermolecular electron transfer (PET) process is thermodynamically allowed and occurs easily through the excited singlet or even triplet state, respectively. This, in turn, allowed the prediction that the tested pyridine compounds in combination with iodonium salt should effectively generate reactive species (e.g., cations, free radicals, or radical-cations).

The nature of the electron transfer process between 2-amino-4,6-diphenyl-pyridine-3-carbonitrile derivatives and iodonium salt was confirmed by fluorescence quenching experiments. Interestingly, it was noticed that the fluorescence of all investigated pyridine derivatives was effectively and rapidly quenched by iodonium salt, which was confirmed by the high values of the Stern–Volmer coefficients (K_{SV}) obtained. The examples of quenching experiments for all pyridine derivatives are in the Supplementary Materials. The quenching rate constant of the fluorescing state of the pyridine derivatives was estimated based on a Stern–Volmer analysis. The obtained quench effect for all pyridine derivatives proved that the photo-induced electron transfer (PET) reaction had occurred. A linear relationship was found for quenching phenomena as the concentration of iodonium salt increased. Moreover, the electron transfer quantum yields from the excited singlet state ($\Phi_{ET(S1)}$) were calculated according to Equation (1) [35]:

$$\Phi_{ET(S1)} = K_{SV}[IOD]/(1+ K_{SV}[IOD]) \quad (1)$$

In order to determine the energy transition (singlet-state energy) between the lowest ground state and the lowest excited state, it was necessary for both normalized absorption and fluorescence spectra of the new sensitizers to overlap. The normalized absorption and fluorescence spectra of all 2-amino-4,6-diphenyl-pyridine-3-carbonitrile derivatives in acetonitrile solvent are presented in the Supplementary Materials. All results are listed in Table 3.

Additionally, the photochemistry of the potential bimolecular photoinitiating systems based on pyridine derivatives and iodonium salt was also investigated by steady-state photolysis. The photostability of pyridine derivatives was investigated using the same experimental conditions under UV-A LED at 365 nm and visible LED at 405 nm, for comparison (Figure 3). All results are included in the Supplementary Materials. As shown in Figure 3, the photolysis of the 2-amino-4,6-diphenyl-pyridine-3-carbonitrile derivatives was considerably faster in the presence of iodonium salt (HIP—diphenyliodonium hexafluorophosphate), e.g., for S4/HIP. This is directly associated with the interaction of pyridine derivatives as photosensitizers for iodonium salt. Photolysis under variable light sources was found to be fastest under UV-A light, while the photolysis rate of S4/HIP under 405 nm was the lowest. This was in line with the lower absorption coefficient at 405 nm rather than at 365 nm. In connection with the above experimental results based on steady-state photolysis, fluorescence quenching, and the favorable free energy of electron transfer (more details are in the Supplementary Materials), a possible mechanism based on the photo-induced electron transfer mechanism (PET) related to the reaction of excited 2-amino-4,6-diphenyl-pyridine-3-carbonitrile derivatives with iodonium salt was proposed.

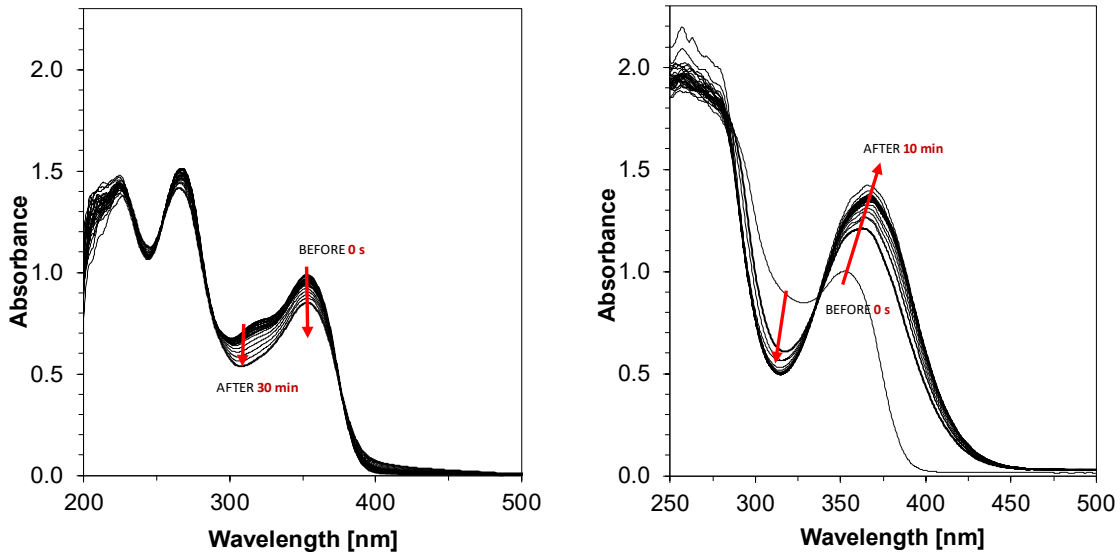

(**a**) (**b**)

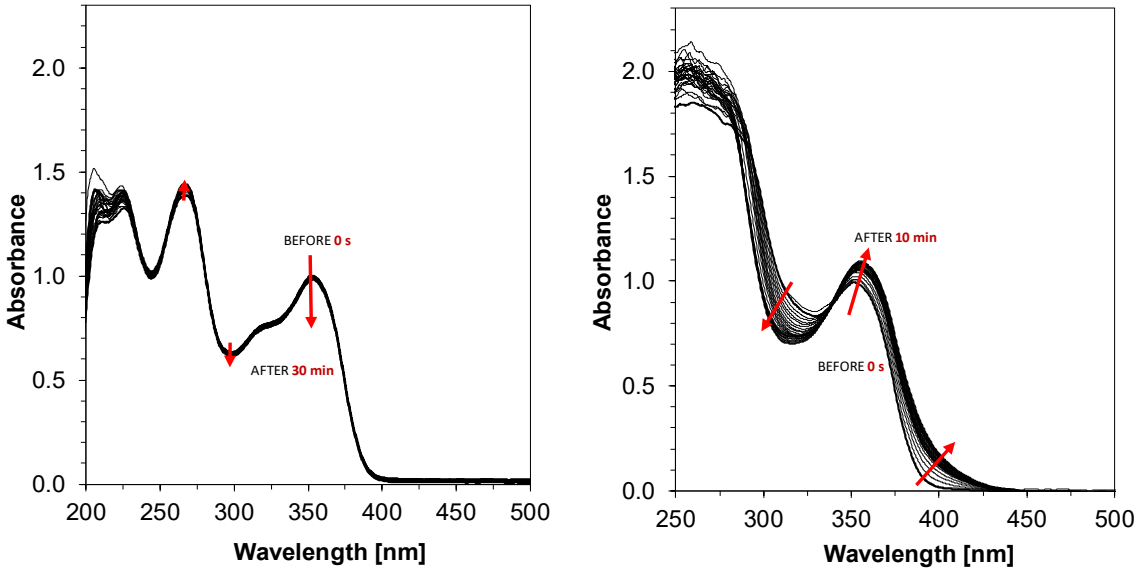

Figure 3. Steady-state photolysis of: (**a**) S4 in acetonitrile under 365 nm (126 mW/cm²) for 30 min; (**b**) S4 with iodonium salt (HIP—diphenyliodonium hexafluorophosphate) in acetonitrile under 365nm (126mW/cm²) for 10 min; (**c**) S4 in acetonitrile under 405 nm (455 mW/cm²) for 30 min; (**d**) S4 with iodonium salt (HIP) in acetonitrile under 405 nm (455 mW/cm²) for 10 min.

2.3. Performance of 2-Amino-4,6-Diphenyl-Pyridine-3-Carbonitrile Derivatives as Photosensitizers in Bimolecular Photoinitiating Systems through Photo-Oxidation Mechanisms for Different Types of Photopolymerization

The light sources utilized in 3D printing techniques are based mainly on UV or visible LEDs with the shortest wavelength of 365 nm. Only triarylsulphonium salts absorb light at this range and can be directly used as initiators for 3D printing with cationic monomers and high light intensity. The absorption spectra of common cationic photoinitiators, compared to the emission spectra of UV-A and visible LEDs, are presented in Figure 4. Iodonium salts exhibit absorption on shorter wavelengths than sulphonium salts. For this, a co-initiator is required to initiate photopolymerization efficiently under longer wavelengths.

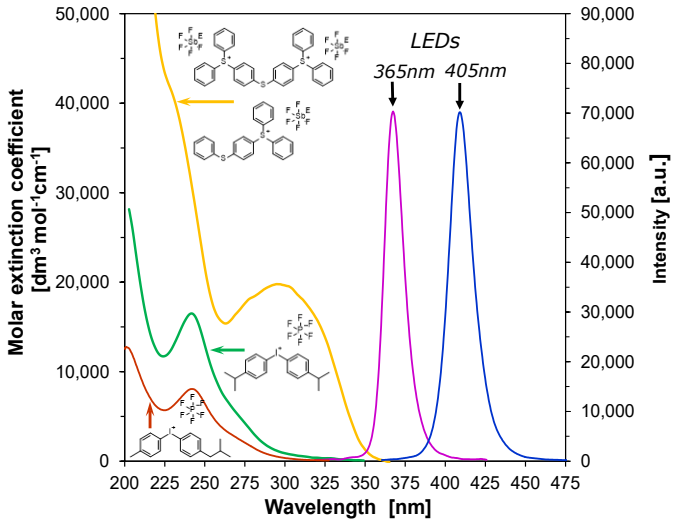

Figure 4. Comparison of absorption spectra of common cationic photoinitiators with emission spectra of 365 nm UV-A LED and visible LED at 405 nm.

2.3.1. Cationic Photopolymerization (CP) of Vinyl and Cycloaliphatic Epoxide Monomers

Cationic photopolymerization of tri(ethylene glycol) divinyl ether (TEGDVE) and cycloaliphatic epoxide monomers 3,4-epoxycyclohexylmethyl 3,4-epoxycyclohexanecarboxylate (CADE) in the presence of the 2-amino-4,6-diphenyl-pyridine-3-carbonitrile derivatives (0.1 wt.%) and iodonium salt (HIP 1.0 wt.%) was carried out under near-UV at 365 nm. The results are shown in Figures 5 and 6. For comparison, iodonium salt (HIP) was tested under the same experimental conditions without any additives. It is noteworthy that diphenyliodonium salt has no initiator ability for cationic photopolymerization under a near-UV light source, which is consistent with the spectroscopic properties of this salt. Based on the measurements of cationic photopolymerization of vinyl monomers (TEGDVE) by real-time FTIR, it can be determined that the induction time for this process ranges from 3 s up to 12 s, and depends on the photosensitizer compound used during the research. Different slope of conversion curves testify to the varied kinetics of photopolymerization depending on the pyridine derivative. Compound S3 exhibits the most favorable kinetics of all investigated compounds in the photopolymerization of TEGDVE, but it does not differ much in the overall conversion of functional groups calculated from FTIR data, because the photopolymerization rate of vinyl monomers is very high (Tables 2 and 3).

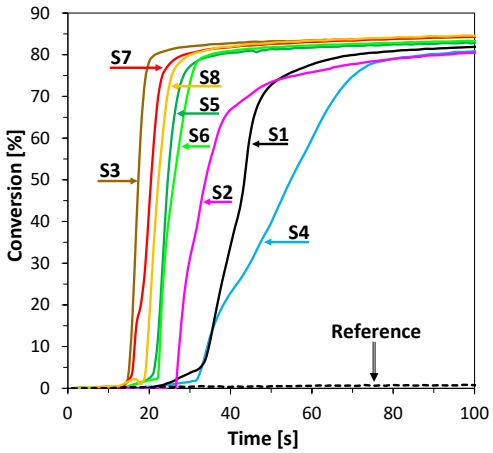

Figure 5. Polymerization profiles of tri(ethylene glycol) divinyl ether (TEGDVE) (vinyl function conversion vs. irradiation time) upon exposure to the UV LED at 365 nm (intensity at the surface of sample 1.59 mW/cm^2) under laminate in the presence of different photoinitiating systems based on diphenyliodonium salt (HIP, 1 wt.%) and 2-amino-4,6-diphenyl-pyridine-3-carbonitrile derivatives(0.1 wt.%). The irradiation starts at t = 10 s.

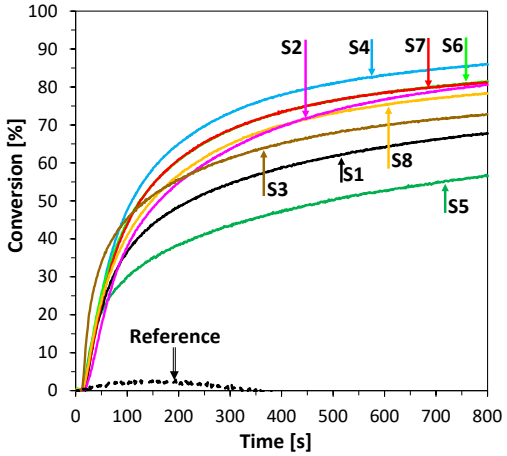

Figure 6. Polymerization profiles of 3,4-epoxycyclohexylmethyl 3,4-epoxycyclohexanecarboxylate (CADE) (epoxy function conversion vs. irradiation time) upon exposure to the UV LED at 365 nm

(intensity at the surface of sample 1.59 mW/cm²) under air in the presence of different photoinitiating systems based on diphenyliodonium salt (HIP, 1 wt.%) and 2-amino-4,6-diphenyl-pyridine-3-carbonitrile derivatives (0.1 wt.%). The irradiation starts at t = 10 s.

2.3.2. Free-Radical Photopolymerization (FRP) of Acrylate Monomers

Photosensitization of iodonium salt using 2-amino-4,6-diphenyl-pyridine-3-carbonitrile derivatives in photoinitiated free-radical polymerization of acrylate monomers trimethylolpropane triacrylate (TMPTA) was also found to be a highly efficient process at 365 nm wavelength. Moreover, the polymerization rate enhancement effect of this process can be easily increased by elevating the power of the LED light sources used. The conversion of double bonds of TMPTA was measured by real-time FTIR and the results are shown in Figure 7. In this case, all compounds, excluding S1 and S2, showed similar kinetics at the beginning of the process but differed in overall conversion. The most promising results were observed for compounds S4 and S7, where polymerization kinetics and final conversion yielded high values. It can be observed that, in this process, the highest conversions were reached by compounds characterized by the lowest value of Gibbs free energy of electron transfer (Tables 2 and 3).

It is worth mentioning that the diphenyliodonium salt alone does not initiate the free-radical photopolymerization of acrylates, indicating the role of 2-amino-4,6-diphenyl-pyridine-3-carbonitrile derivatives as photosensitizers of iodonium salt through the mechanism of photo-oxidizable sensitization of this salt under near-UV light.

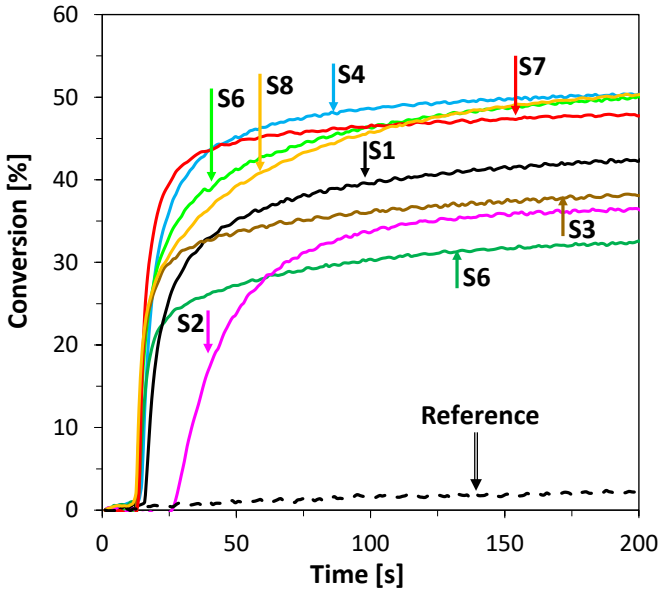

Figure 7. Conversion of double bonds of trimethylolpropane triacrylate (TMPTA) recorded during free-radical photopolymerization with photoinitiating systems (PISs) based on (HIP (1 wt.%) and 2-amino-4,6-diphenyl-pyridine-3-carbonitrile derivatives (0.1 wt.%) under UV-LED 365 nm (intensity at the surface of sample 1.59 mW/cm²) irradiation. The irradiation starts at t = 10 s.

2.3.3. Thiol-Ene Photopolymerization (TEP) of Methacrylate and Thiol Monomers

Photo-induced thiol-ene reactions exhibit the characteristics of both photopolymerization and click reactions, such as spatial and temporal control, high selectivity, insensitivity to oxygen or water, and high yield with no formation of by-products [36]. Due to the unique features of thiol-ene photopolymerization, such as low shrinkage stress and the yielding of homogeneous networks, this type of reaction is very promising for 3D-printing [37,38]. Therefore, thiol–ene resin has been applied to the fabrication of devices via 3D printing [39,40]. For this reason, it was decided to study the suitability of the developed bimolecular photoinitiating systems consisting of 2-amino-4,6-diphenyl-pyridine-3-carbonitrile derivatives and iodonium salt during thiol-ene photopolymerization of methacrylate monomer trimethylopropane trimethacrylate (TMPTA) and

trimethylolpropane tris(3-mercaptopropionate) (MERCAPTO) upon exposure to near-UV light at 365 nm. The excellent conversion versus irradiation time curves for the thiol-ene polymerization under air in the presence of the investigated bimolecular system is shown in Figures 8 and 9.

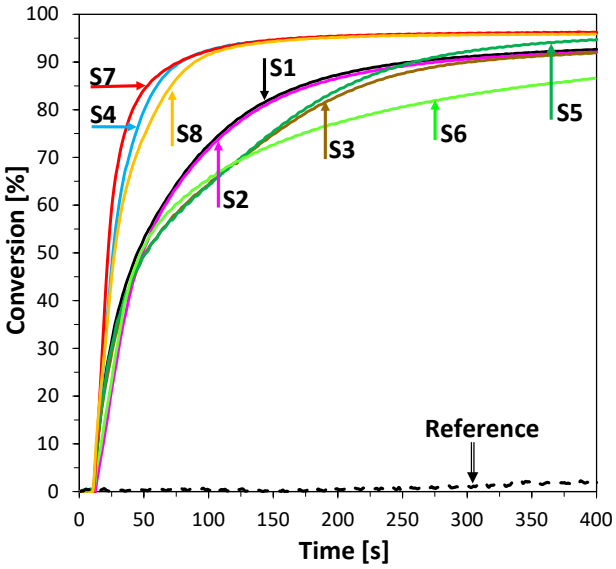

Figure 8. Conversion of double bonds of trimethylolpropane trimethacrylate (TMPTMA) recorded during thiol–ene photopolymerization with PISs based on HIP (1 wt.%) and 2-amino-4,6-diphenyl-pyridine-3-carbonitrile derivatives (0.1 wt.%) under UV-LED 365 nm (intensity at the surface of sample 1.59 mW/cm^2) irradiation. The irradiation starts at t = 10 s.

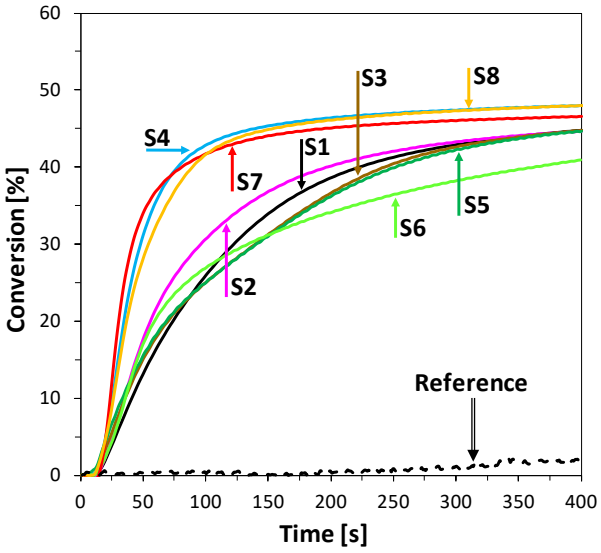

Figure 9. Conversion of SH bonds of trimethylolpropane tris(3-mercaptopropionate) MERCAPTO recorded during thiol-ene photopolymerization with PISs based on HIP (1 wt.%) and 2-amino-4,6-diphenyl-pyridine-3-carbonitrile derivatives (0.1 wt.%) under UV-LED 365 nm (intensity at the surface of sample 1.59 mW/cm^2) irradiation. The irradiation starts at t = 10 s.

The final monomer conversion after only 400 s of irradiation is summarized in Table 3. During the thiol–ene process, the values of conversion of the methacrylate monomer reached 95%, while the conversion of thiols was at 47% (Table 3). The addition of the thiol monomer yielded high conversion values for the methacrylic monomer through the elimination of negative oxygen influence.

Table 3. Functional group conversions using bimolecular photoinitiating systems. (A) Photo-oxidation mechanisms of photopolymerization: diphenyliodonium hexafluorophosphate (HIP 1 wt.%) and 2-amino-4,6-diphenyl-pyridine-3-carbonitrile derivatives (0.1 wt.%) as photosensitizers; (B) photo-reduction mechanisms: 4-(dimethylamino)benzoate (EDB 1.5 wt.%) and 2-amino-4,6-diphenyl-pyridine-3-carbonitrile derivatives (0.1 wt.%).

Acronim	Photo-Oxidation Mechanisms of Photopoly Merization					Photo-Reduction Mechanisms
	Cationic Polymerization		Free Radical Polymerization	Thiol–ene Polymerization		Free Radical Polymerization
	[%] CADE Monomer after 800 s	[%] TGDVE Monomer after 100 s	[%] TMPTA Monomer after 200 s	[%] TMPTMA Monomer after 200 s	[%] MERCAPTO Monomer after 400 s	[%] TMPTA Monomer after 200 s
	@365 nm ~1.59 mW/cm²	@365 nm ~1.59 mW/cm²	@365 nm ~1.59 mW/cm²	@365 nm ~1.59 mW/cm²		@405 nm ~6 mW/cm²
S1	67.7	81.9	42.5	92.6	44.8	2.7
S2	80.6	80.5	36.3	92.1	44.7	43.2
S3	72.9	84.3	38.2	91.9	44.8	46.1
S4	86.0	80.9	50.3	96.0	47.9	38.6
S5	56.6	82.9	32.5	94.7	44.6	44.6
S6	81.5	83.3	49.9	86.6	40.9	48.5
S7	81.1	84.3	47.8	96.2	48.5	39.2
S8	78.2	84.6	50.2	95.8	48.0	34.9

2.4. Performance of 2-Amino-4,6-Diphenyl-Pyridine-3-Carbonitrile Derivatives as Photosensitizers in Bimolecular Photoinitiating Systems through Photo-Reduction Mechanisms for Free-Radical Photopolymerization

During this research, it was found that bimolecular systems based on 2-amino-4,6-diphenyl-pyridine-3-carbonitrile derivatives and diphenyliodonium salt are quite efficient in both photo-oxidation and photo-reduction processes. The process responsible in the photo-reduction mechanism was the electron transfer from amine to the excited state of a pyridine chromophore. Using this type of photo-reductive process, free-radical photopolymerization of trimethylolpropane triacrylate was carried out in the presence of 2-amino-4,6-diphenyl-pyridine-3-carbonitrile derivatives as electron acceptors and ethyl 4-(dimethylamino)benzoate (EDB) as the co-initiator. Therefore, it was found that the combination of EDB amine and the investigated derivatives exhibited the ability to initiate photo-induced free-radical polymerization as type II free-radical bimolecular initiators. The typical methacrylate function conversion-time profiles are given in Figure 10. The highest final conversions (around 45%) were obtained for S3/EDB systems (Table 3).

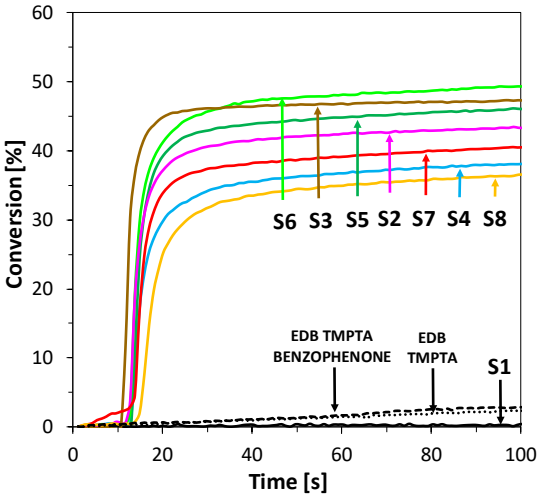

Figure 10. Conversion of double bonds of TMPTA recorded during free-radical photopolymerization with ethyl 4-dimethylaminobenzoate (EDB, 1.5% *w*/*w*) and 2-amino-4,6-diphenyl-pyridine-3-carbonitrile derivatives (0.2% *w*/*w*) under visible-LED 405 nm (6 mW/cm^2) irradiation. The irradiation starts at t = 10 s.

According to the ΔG_{ET} values summarized in Table 4, electron transfer from EDB to 2-amino-4,6-diphenylpyridine-3-carbonitrile derivatives is feasible and thermodynamically favorable for all pyridine derivatives from singlet and triplet excited stages. The interaction between amine and all pyridine derivatives has been proven by fluorescence quenching experiments (see Supplementary Materials). For free energy changes, however, the photo reduction process is less favorable than the photo oxidation process (Tables 2 and 4). This interaction is confirmed by experimental kinetic data.

Table 4. Electrochemical and thermodynamically properties of investigated in the presence of different photoinitiating systems based on EDB (1.5% *w*/*w*) and 2-amino-4-methyl-6-phenyl-benzene-1,3-dicarbonitrile derivatives (0.1% *w*/*w*) in terms of their use in photo-reduction mechanism in light induces electron transfer process.

Abb.	$E_{red}^{1/2}$ (mV)	$E_{00(S1)}$ (eV)	$E_{00(T1)}$ (eV)	$\Delta G_{ET(S1)}$ (eV)	$\Delta G_{ET(T1)}$ (eV)	K_{SV} (M^{-1})	$\Phi_{ET(S1)}$
S1	−1753	311	2.57	−0.41	0.24	62.59	0.45
S2	−1477	297	2.46	−0.54	0.08	13.28	0.15
S3	−1470	290	2.45	−0.48	0.09	33.43	0.30
S4	−1433	304	2.57	−0.56	0.02	24.97	0.24
S5	−1737	308	2,46	−0.40	0.34	24.48	0.24
S6	−1719	302	2.51	−0.35	0.28	23.27	0.23
S7	−1790	307	2.54	−0.33	0.32	21.97	0.22
S8	−1771	306	2.52	−0.34	0.32	22.57	0.23

$E_{red}^{1/2}$—the electrochemically determined reduction half-wave potentials (vs. Ag/AgCl); $E_{00(S1)}$—the excitation energy of the photosensitizer, which is referred to as singlet excitation energy; $E_{00(T1)}$—the triplet state energies were calculated on the basis of the uM06/6-31G level of theory; $\Delta G_{ET(S1)}$—the enthalpy of free electron transfer from singlet state between EDB and pyridine derivatives (oxidation potential of the electron donor; −1.058 V for amine EDB (vs. Ag/AgCl) [41]); $\Delta G_{ET(T1)}$—the enthalpy of free electron transfer from triplet state between EDB and pyridine derivatives $\Phi_{ET(S1)}$ electron transfer quantum yields: $\Phi_{ET} = K_{SV}[EDB]/(1 + K_{SV}[EDB])$ with concentration of amine [EDB] = 0.086 mol/dm^3.

2.5. Performance of 2-Amino-4,6-Diphenyl-Pyridine-3-Carbonitrile Derivatives as Visible Photosensitizers in Bimolecular Photoinitiating Systems for 3D Printing Processes

In order to test the scope of applicability of bimolecular photoinitiating systems we examined the possibility of using them for photopolymerization in the visible light range. For this purpose, free-radical and cationic photopolymerization processes with the proposed photoinitiating systems under two different light sources using the photo-DSC technique were carried out. At the beginning, photo-DSC measurements were conducted with broad band medium pressure mercury lamp (MPM) OmniCure S2000 (from Excelitas Technologies®, Ontario, Canada) with a visible filter (400–500 nm). The second source of light was the narrow band visible LED (Bluepoint LED eco light source, from Dr. Hönle AG, Germany) with a maximum emission of 405 nm. An LED source of light was used for the investigation of initiating system properties at conditions known from modern 3D printers equipped with 405 nm LEDs or 405 nm laser diodes. Trimethylopropane triacrylate (TMPTA) and 3,4-epoxycyclohexylmethyl 3,4-epoxycyclohexanecarboxylate (CADE) were selected as the model monomers, because they are representative of acrylate and epoxy monomers, most often used for coating formulations cured by the free-radical and cationic polymerization mechanisms respectively.

Photo-DSC is capable of measuring any emitted heat during the photopolymerization process. This is directly proportional to the number of groups reacting in the photopolymerization process. Comparing the heat flow of the reaction recorded by the photo-DSC method, released during the photopolymerization process, with the theoretical heat of reaction ($\Delta H_{\text{teoretical}}$) of all monomer functional groups, the molecular weight and density, and the conversion of monomers during the irradiation of the sample can be determined. The conversion of monomer ($C_{\text{photo-DSC}}$) was calculated by Equation (2):

$$C_{\text{photo-DSC}} = \frac{M}{f \cdot \Delta H_0} \cdot \int_{t_o}^{t} \frac{H(t)}{m_p} dt \quad (2)$$

where M is molecular mass of monomer [g/mol]; f is functionality of monomer; ΔH_0 is enthalpy of polymerization [J/mol] (calculated on one functional group); H is heat flow [W]; and m_p is sample mass [g].

Raw heat flow data recorded during measurements can also be converted into polymerization rate profiles, which exhibit the nature of photopolymerization kinetics. The highest value of photopolymerization rate denotes the highest speed of photopolymerization reaction. Consequently, the rate of polymerization (R_p), which is the number of monomers being consumed over the total number of monomers per time, can be determined according to Equation (3):

$$R_p \approx 1000 \cdot \frac{d_m}{\Delta H_o} \cdot \left(\frac{H}{m_p} \right) \quad (3)$$

where d_m is density of composition [g/mL], ΔH_0 is enthalpy of polymerization [J/mol] (calculated on one functional group), H is heat flow [W], and m_p is sample mass [g]. By integrating the area under the rate of polymerization graph, the conversion of monomers was obtained.

The rate profiles for the cationic and free-radical photopolymerization of the formulations involving pyridine derivatives in combination with iodonium salt as photoinitiating systems exhibited the expected nature and course, as reported in real-time FTIR experiments under a UV-A source of light with a maximum emission of 365 nm. The polymerization ratio during photopolymerization under a narrow LED source of light with emission at 405 nm, in most cases, was lower than under the broad band visible MPM lamp with the 400–500 nm filter. The results of this experiment are shown in Figures 11–18.

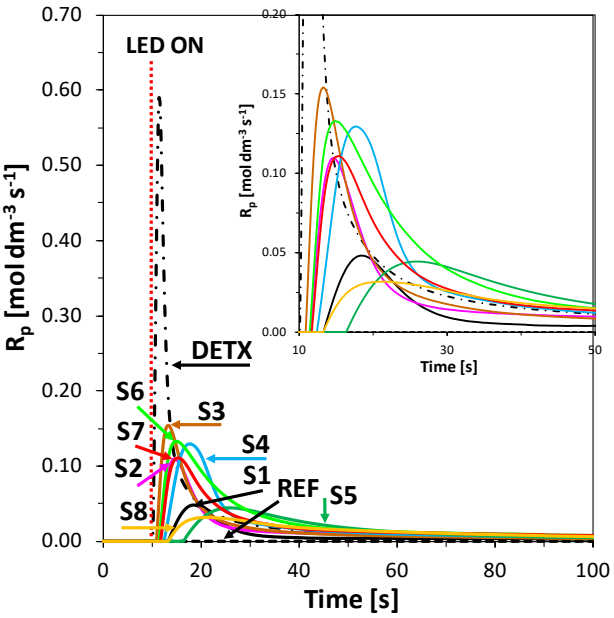

Figure 11. Polymerization rate profiles for photopolymerization of CADE with HIP (1 wt.%) and 2-amino-4,6-diphenyl-pyridine-3-carbonitrile derivatives (0.1 wt.%) under MPM lamp with 400-500 nm filter (intensity at the surface of sample 75 mW/cm^2) irradiation, calculated from photo-DSC data. The irradiation starts at t = 10 s.

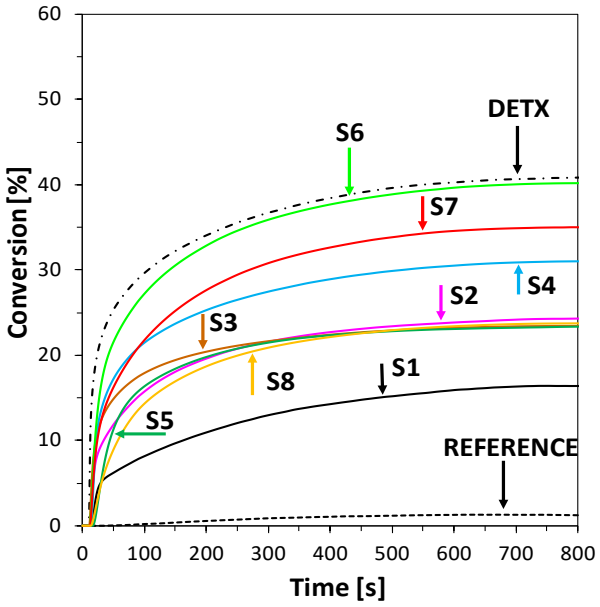

Figure 12. Profiles of CADE epoxy groups conversion with HIP (1 wt.%) and 2-amino-4,6-diphenyl-pyridine-3-carbonitrile derivatives (0.1 wt.%) under MPM lamp with 400–500 nm filter (intensity at the surface of sample 75 mW/cm^2) irradiation, calculated from photo-DSC data. The irradiation starts at t = 10 s.

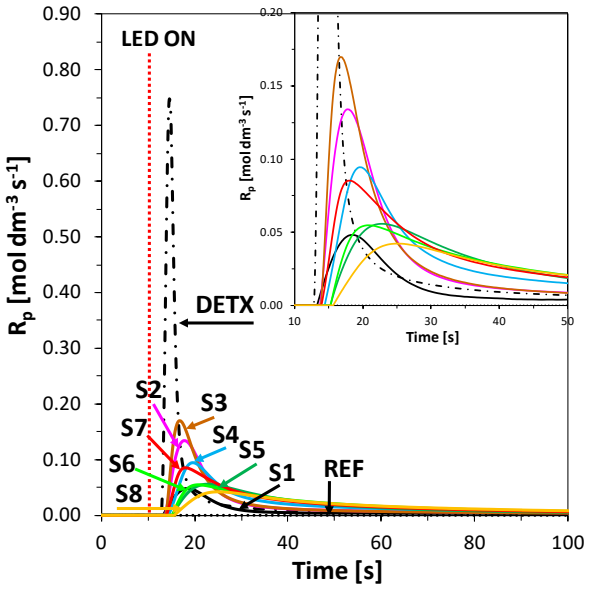

Figure 13. Polymerization rate profiles for photopolymerization of CADE with HIP (1 wt.%) and 2-amino-4,6-diphenyl-pyridine-3-carbonitrile derivatives (0.1 wt.%) under 405 nm LED (intensity at the surface of sample 25 mW/cm²) irradiation, calculated from photo-DSC data. Irradiation begins at t = 10 s.

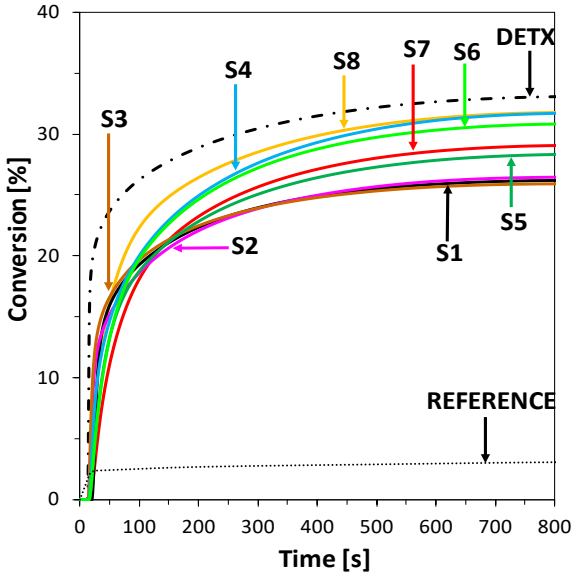

Figure 14. Profiles of CADE epoxy group conversion with HIP (1 wt.%) and 2-amino-4,6-diphenyl-pyridine-3-carbonitrile derivatives (0.1 wt.%) under 405 nm LED (intensity at the surface of sample 25 mW/cm²) irradiation, calculated from photo-DSC data. Irradiation begins at t = 10 s.

Moreover, a comparison of the maximum polymerization rates and the final conversion rates for all sensitizers are shown in Table 5. Further, using these new photoinitiating systems during the irradiation of cycloaliphatic epoxide formulation by visible sources of light can initialize the photopolymerization of epoxy groups efficiently, as observed in Figures 11 and 12. The worst photopolymerization rate was observed when compound 2-amino-4,6-diphenyl-pyridine-3-carbonitrile (S1) was used as a photosensitizer. This was correlated with the absorption characteristics of this compound and one of the lowest molar extinction coefficients at the 405 nm wavelength, and the highest oxidation potential. Conversely,

cationic composition with 2-amino-4-(4-cyanophenyl)-6-(4-methylthiophenyl)-pyridine-3-carbonitrile (S3) shows the highest value of Rp, which means that photopolymerization speed with this composition is the best and is also related to the spectroscopic properties of this compound under the visible range (Table 5).

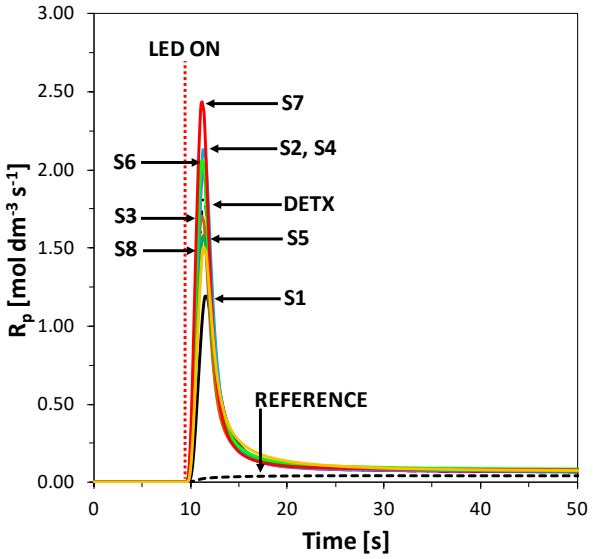

Figure 15. Polymerization rate profiles for photopolymerization of TMPTA with HIP (1 wt.%) and 2-amino-4,6-diphenyl-pyridine-3-carbonitrile derivatives (0.1 wt.%) under MPM lamp with 400–500 nm filter (intensity at the surface of sample 75 mW/cm^2) irradiation, calculated from photo-DSC data. The irradiation starts at t = 10 s.

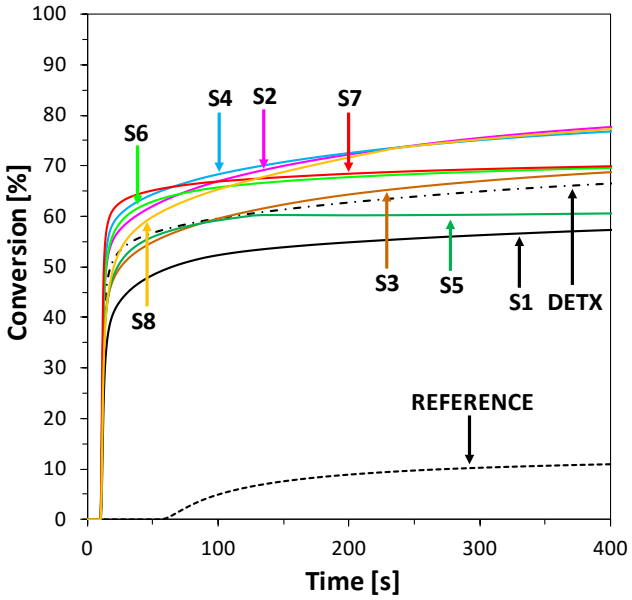

Figure 16. Profiles of TMPTA double bond conversion with HIP (1 wt.%) and 2-amino-4,6-diphenyl-pyridine-3-carbonitrile derivatives (0.1 wt.%) under MPM lamp with 400–500 nm filter (intensity at the surface of sample 75 mW/cm^2) irradiation, calculated from photo-DSC data. The irradiation starts at t = 10 s.

Compositions with bimolecular photoinitiating systems based on S1–S8 and iodonium salt (HIP) in free-radical formulation with TMPTA exhibited favorable kinetics and high conversion of functional groups. The value of monomer conversion for compound photoinitiating systems based on S2, S4, and S6–8 is even better than for commercial photosensitizer 2,4-diethyl-9H-thioxanthen-9-one (DETX). The best conversions during the photopolymerization

process under a visible LED source and broad band lamp with a 400–500 nm filter were observed for compounds 2-amino-4-(4-methylthiophenyl), 6-phenyl pyridine-3-carbonitrile (S4), and 2-amino-4-(4-methoxyphenyl)-6-(4-methylthiophenyl)-pyridine-3-carbonitrile (S8). Composition with compound 2-amino-4-(4-methylthiophenyl)-6-(4-methoxyphenyl)-pyridine-3-carbonitrile (S7) showed great R_p value, which means that polymerization speed at formulation in this composition was the best.

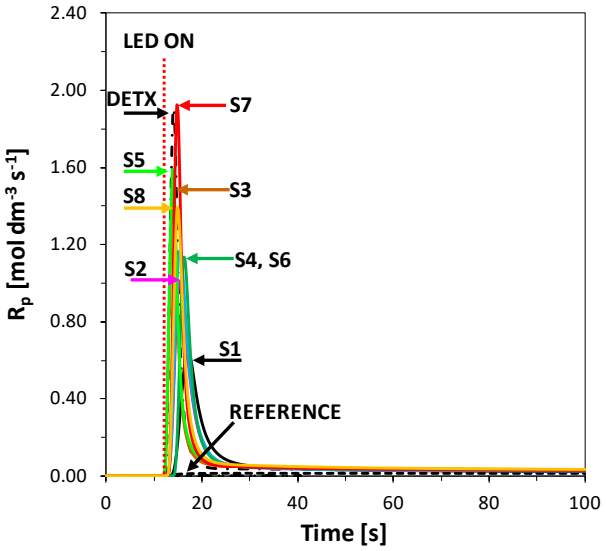

Figure 17. Polymerization rate profiles for photopolymerization of TMPTA with HIP (1 wt.%) and 2-amino-4,6-diphenyl-pyridine-3-carbonitrile derivatives (0.1 wt.%) under 405 nm LED (intensity at the surface of sample 25 mW/cm^2) irradiation, calculated from photo-DSC data. The irradiation starts at t = 10 s.

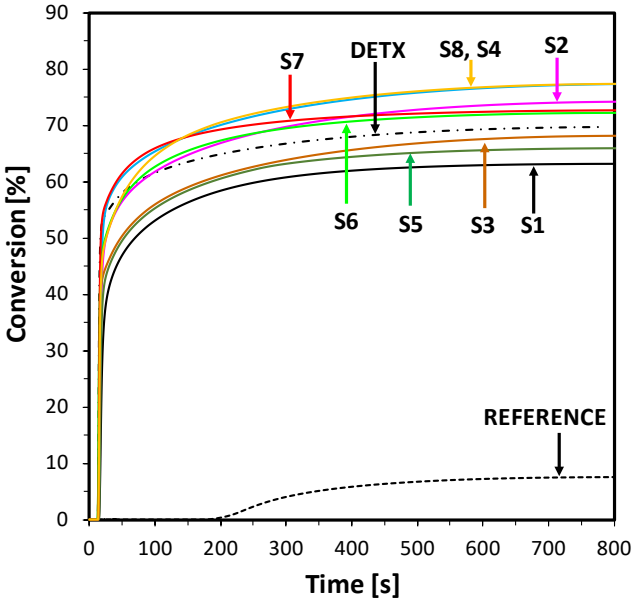

Figure 18. Profiles of TMPTA double bond conversion with HIP (1 wt.%) and 2-amino-4,6-diphenyl-pyridine-3-carbonitrile derivatives (0.1 wt.%) under 405 nm LED (intensity at the surface of sample 25 mW/cm^2) irradiation, calculated from photo-DSC data. The irradiation starts at t = 10 s.

Table 5. Kinetic parameters obtained during cationic and free-radical photopolymerization processes using bimolecular photoinitiating systems based on 2-amino-4,6-diphenyl-pyridine-3-carbonitrile derivatives (0.1 wt.%) with diphenyliodonium salts (HIP, 1 wt.%).

System	Source of Light	Induction Time (s)	Peak Max. Time (s)	$R_{p\text{-}max}$ (mol/dm³s)	ΔH (mJ/mg)	$C_{photo\text{-}DSC}$ (%)
Cationic photopolymerization						
S1	LED 405 nm	3.0	18.4	0.0482	120.1	16.4
	MPM lamp 400–500 nm	0.7	18.6	0.0482	124.8	16.4
S2	LED 405 nm	3.3	14.6	0.1341	185.1	25.6
	MPM lamp 400–500 nm	0.3	12.0	0.1096	185.1	24.3
S3	LED 405 nm	3.5	13.2	0.1698	179.5	25.4
	MPM lamp 400–500 nm	0.3	12.2	0.1541	178.4	23.4
S4	LED 405 nm	2.5	17.6	0.0944	235.0	31.7
	MPM lamp 400–500 nm	0.8	18.1	0.1295	236.2	31.0
S5	LED 405 nm	3.4	21.5	0.0558	208.2	28.3
	MPM lamp 400–500 nm	1.4	23.8	0.0444	174.0	23.3
S6	LED 405 nm	3.6	14.9	0.0548	307.6	30.8
	MPM lamp 400–500 nm	0.2	12.3	0.1329	305.9	40.2
S7	LED 405 nm	2.0	15.2	0.0853	257.8	31.8
	MPM lamp 400–500 nm	0.2	18.0	0.1108	266.5	35.0
S8	LED 405 nm	2.8	21.5	0.0422	180.4	29.1
	MPM lamp 400–500 nm	0.2	21.5	0.0318	180.8	23.7
Free-radical photopolymerization						
S1	LED 405 nm	3.2	12.0	0.6411	366.6	63.1
	MPM lamp 400–500 nm	3.0	12.1	1.1921	342.9	57.3
S2	LED 405 nm	2.6	18.2	1.0104	430.8	74.2
	MPM lamp 400–500 nm	3.3	12.0	1.9688	469.6	77.7
S3	LED 405 nm	2.1	12.6	1.4591	395.5	68.1
	MPM lamp 400–500 nm	3.6	12.5	1.7048	414.1	68.8
S4	LED 405 nm	2.3	16.8	1.1681	449.0	77.3
	MPM lamp 400–500 nm	4.1	12.2	2.1288	461.9	76.8
S5	LED 405 nm	3.9	17.2	1.1345	382.6	65.9
	MPM lamp 400–500 nm	0.1	12.8	1.5791	356.2	60.6
S6	LED 405 nm	2.0	13.5	1.5901	419.1	72.2
	MPM lamp 400–500 nm	0.3	12.9	2.0590	409.5	69.6
S7	LED 405 nm	2.7	13.5	1.9246	421.7	72.7
	MPM lamp 400–500 nm	0.2	12.9	2.4357	412.5	69.9
S8	LED 405 nm	2.8	11.5	1.3935	449.1	77.3
	MPM lamp 400–500 nm	0.3	11.6	1.5053	467.1	77.3

2.6.Performance of New Visible Bimolecular Photoinitiating Systems for 3D Printing Experiments

The known physicochemical properties of the new photoinitiating systems, based on pyridine derivatives and iodonium salt, have directed the investigation towards the consideration of the stereolithography process. At the beginning, formulations were poured into a 20 × 10 × 2 mm vat 3D printed from polylactide and placed in the middle of the working table of an NEJE laser engraver.

The software delivered with this printer does not allow the user to directly control the power of the laser. Adjustable parameters are, in this case, the time of illumination of the spot on the print in the range 10–100 μs. During preparation of the sketch for printing, the software divided the drawing into tiny spots, which would be exposed to the laser beam for a programmed period of time. Spots formed during the printing process using vinyl monomer (TEGDVE) or cycloaliphatic epoxide monomer (CADE) are clearly visible in Figure 19. In the case of the printing process using the bimolecular initiating system, similar results were observed for formulations S4, S5, S6, S7, and S8. In the case of other derivatives of 2-amino-4,6-diphenyl-pyridine-3-carbonitrile, even at 100 μs of illumination, the obtained shapes lost their resolution or the printed inscription was poorly polymerized.

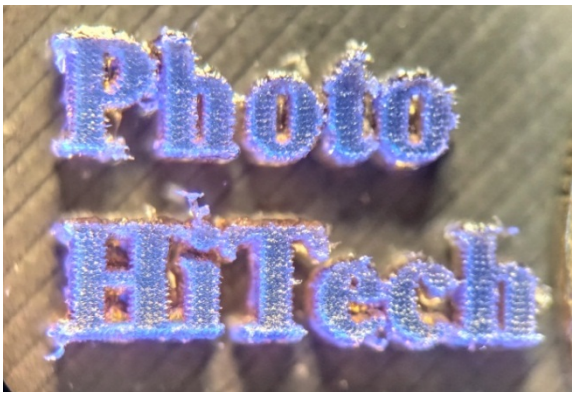

(**A1**)

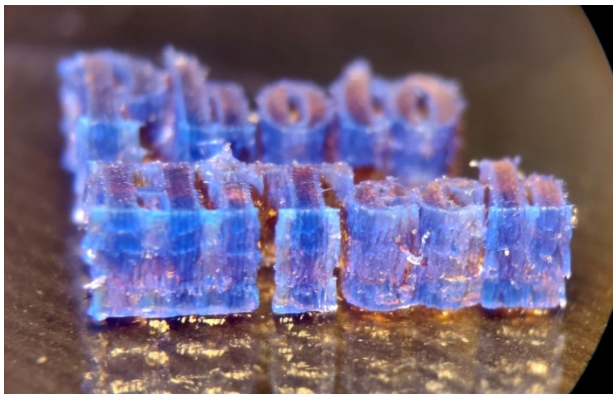

(**A2**)

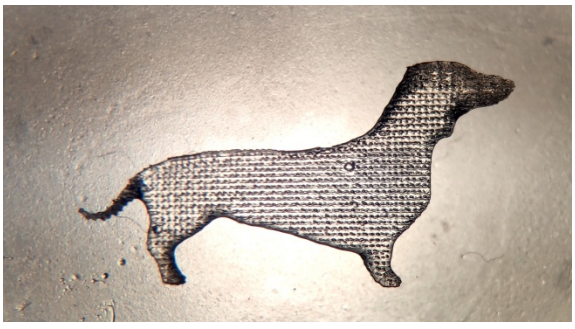

(**B1**)

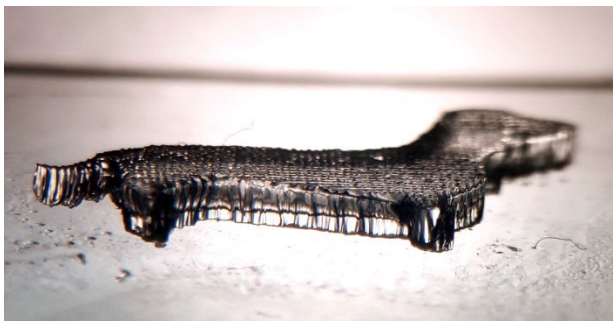

(**B2**)

Figure 19. Micrography of (**A**) object "Photo HiTech" print obtained from purely cationic photosensitive formulations based on vinyl monomer (TEGDVE) with S8/HIP (0.5%/1.0% *w*/*w*) photoinitiating system; (**A1**) view from the top under a UV-LED source of light with a maximum emission at 365 nm; (**A2**) side view at 45° under a UV-LED source of light with a maximum emission at 365 nm. (**B**) Object "dog" print obtained from purely cationic photosensitive formulations based on cycloaliphatic epoxide monomer (CADE) with S8/HIP (0.5%/1.0% *w*/*w*) photoinitiating system photoinitiating system; (**B1**) view from the top in daylight; (**B2**) side view at 45° in daylight.

In order to examine the properties of the obtained purely cationic photosensitive formulations in a 3D printer with a continuous laser beam and modulated laser power, a home-made Computerized Numerical Control (CNC) machine with a 405 nm laser head was used. To begin with, compositions were applied by an industrial applicator calibrated at 90 μm of layer height on the polished glass surface, and cured with laser power of 300 mW. The speed of the laser head was

set to 20 mm/s. In these settings, it was possible to print shapes with a maximum resolution of 100 µm. As can be observed in Figure 20, composition with the commercial photosensitizer DETHX was cured by laser beam. The composition was over-cured around the path followed by the laser. This photo shows the disadvantages of cationic photopolymerization for 3D printing processes—the migration of protic acid from the illuminated area into the uncured composition, which led to polymerization all around the lit area. This phenomenon can be overcome by application of specific compounds (light blocker or UV blocker), which are able to capture free protic acid and absorb light dissipated into the cured composition. Such compounds are derivatives of 2-amino-4,6-diphenyl-pyridine-3-carbonitrile and dependent on the activity as photosensitizer, different derivatives present different influence on resolution of photocured material. Picture 2B shows the application effect of poorly active compound S1 into the photocurable formulation due to the low polymerization ratio in photopolymerization of cycloaliphatic epoxy resin that is highly uncured. On the other hand, the results shown in Photograph 2B present perfectly laser-light cured resin when compounded with proper activity, as in photosensitizer S8, and when a free acid scavenger is present in composition. Some of the deformation of 3D printing objects originated in the washing process, resulting in the poor adhesion of prints to polished glass.

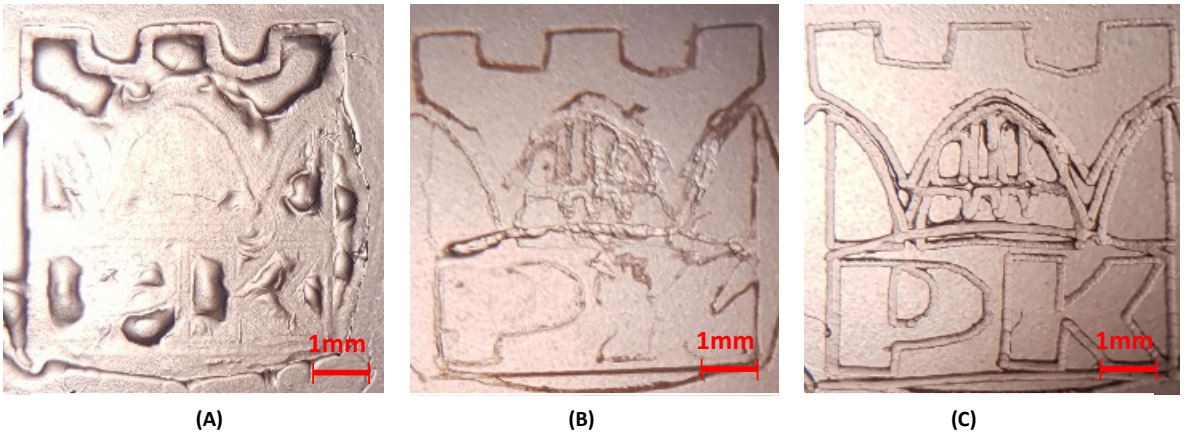

Figure 20. Micrography of the print obtained from cycloaliphatic epoxide monomer (CADE) with a bimolecular photoinitiating system based on; (**A**) DETHX/HIP (0,1%/1% *w*/*w*), (**B**) S1/HIP (1%/1% *w*/*w*), (**C**) S8/HIP (1%/1% *w*/*w*).

Multilayer printing experiments were conducted by pouring liquid resin into a PLA vat with dimensions of 20 × 30 × 10 mm. Such samples were cured with a power of 1500 mW for the first layer and 750 mW for every subsequent layer. The speed of the laser head was set to 20 mm/s. In this case, compositions with compounds S4, S5, S6, S7, and S8 had similar resolution and printing properties. The results of this experiment are shown in Figure 21. Prints obtained with the DETX co-initiator were over-cured and, as a result, lost their resolution.

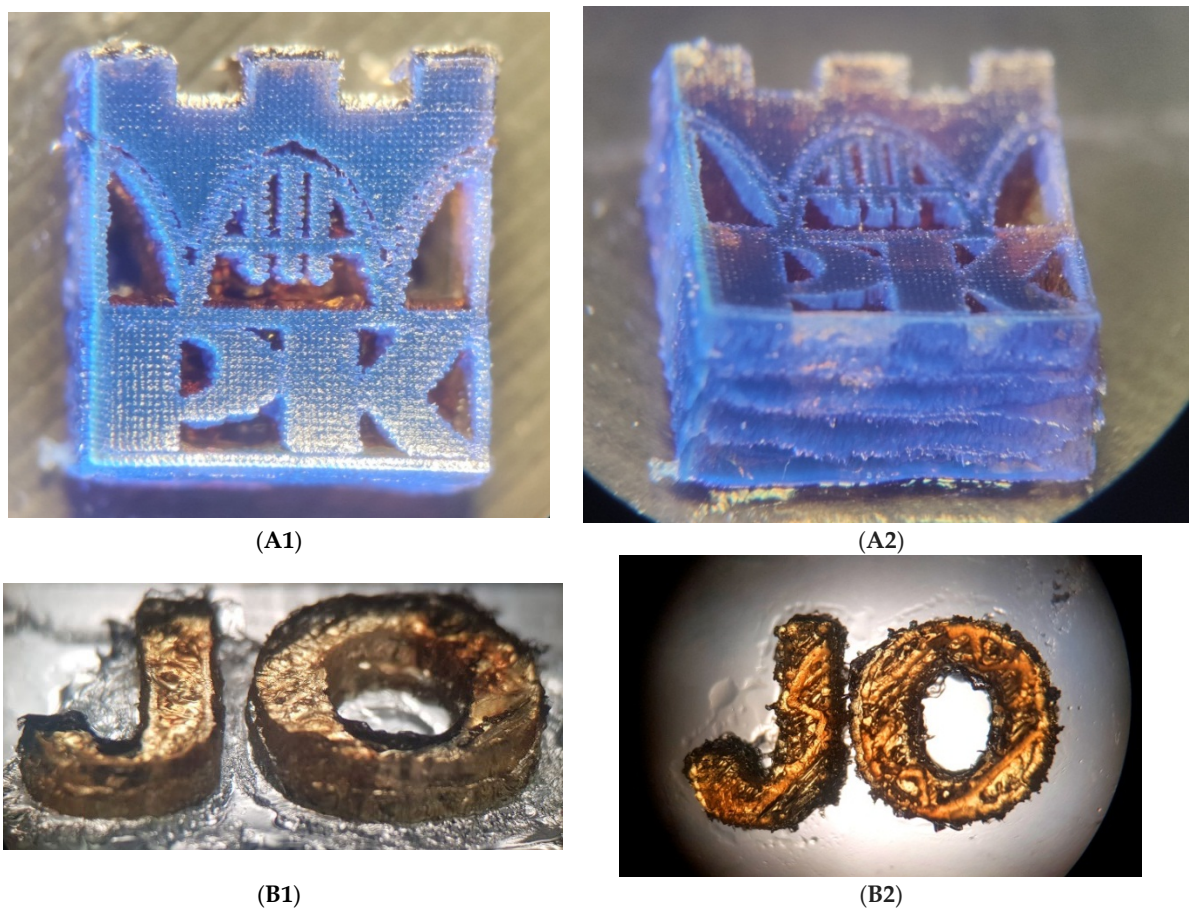

(**A1**) (**A2**)

(**B1**) (**B2**)

Figure 21. Micrography of (**A**) logo of Cracow University of Technology. The print was obtained from purely cationic photosensitive formulations based on vinyl monomer (TEGDVE) with S8/HIP (0.5%/1.0% *w*/*w*) photoinitiating system. (**A1**) View from the top under a UV-LED source of light with a maximum emission at 365nm; (**A2**) side view at 45° under a UV-LED source of light with a maximum emission at 365nm. (**B**) Object showing the initials "JO"; (**B1**) print obtained from purely cationic photosensitive formulations based on cycloaliphatic epoxide monomer (CADE) with an initiating system consisting of a double layer print from the formulation of CADE monomer with S8/HIP (1%/1% *w*/*w*), mono-layer height 1 mm; (**B2**) top view of 3D print.

3. Experimental Section

3.1. Materials

Triethylene glycol divinyl ether (TEGDVE, from Sigma-Aldrich, St. Louis, MO, USA) and 3,4-epoxycyclohexylmethyl 3,4-epoxycyclohexanecarboxylate (CADE, commercial name S105, Lambson Ltd, Wetherby, UK) were applied as a model vinyl ether monomer and cycloaliphatic epoxide monomer, respectively, for the compositions cured by cationic photopolymerization. For the role of cationic photoinitiator, diphenyliodonium hexafluorophosphate (HIP, from Alfa Aesar, Haverhill, MA, USA) was used. Ethyl 4-(dimethylamino)benzoate (EDB) for oxidative reduction cycle experiments was purchased from Sigma-Aldrich, Germany. Trimethylopropane triacrylate (TMPTA, from Sigma-Aldrich, St. Louis, MO, USA) was employed as an acrylate monomer polymerized by a free-radical mechanism. Further, trimethylopropane trimethacrylate (TMPTMA, from Sigma-Aldrich, St. Louis, MO, USA) and trimethylopropane tris(3-mercaptopropionate) (MERCAPTO, Sigma-Aldrich, St. Louis, MO, USA) were utilized as methacrylate and thiol monomers for the compositions polymerized by the thiol–ene mechanism.

For the bimolecular initiating systems, a series of derivatives of 2-amino-4,6-diphenyl-pyridine-3-carbonitrile combined with HIP were chosen. These derivatives were:

2-amino-4,6-diphenyl-pyridine-3-carbonitrile (S1),
2-amino-4-(4-methylthiophenyl)-6-(4-cyanophenyl)-pyridine-3-carbonitrile (S2),
2-amino-4-(4-cyanophenyl)-6-(4-methylthiophenyl)-pyridine-3-carbonitrile (S3),
2-amino-4-(4-methylthiophenyl)-6-phenylpyridine-3-carbonitrile (S4),
2-amino-4-phenyl-6-(4-methylthiophenyl)pyridine-3-carbonitrile (S5),
2-amino-4,6-bis(4-methylthiophenyl)--pyridine-3-carbonitrile (S6),
2-amino-4-(4-methylthiophenyl)-6-(4-methoxyphenyl)-pyridine-3-carbonitrile (S7),
2-amino-4-(4-methoxyphenyl)-6-(4-methylthiophenyl)-pyridine-3-carbonitrile (S8)

The synthesis and physicochemical properties of the derivatives of 2-amino-4,6-diphenyl-pyridine-3-carbonitrile are provided in the Supplementary Materials. The synthesis and physicochemical properties of the pyridine derivatives are also described in the Supplementary Materials. The structures of the compounds are shown in Table 6.

Table 6. Structures of investigated photosensitizers for photopolymerization processes.

Structures of 2-Amino-4,6-Diphenyl-Pyridine-3-Carbonitrile Derivatives		
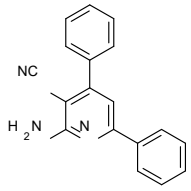	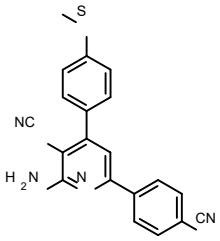	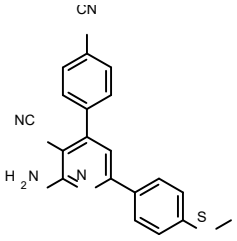
S1	S2	S3
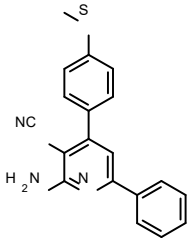	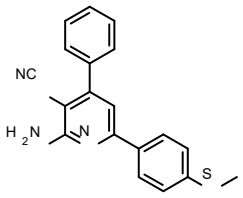	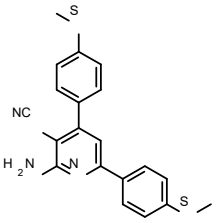
S4	S5	S6
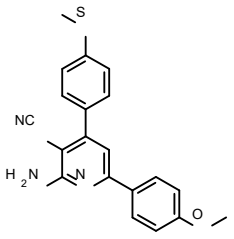		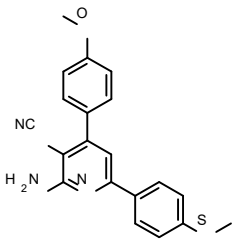
S7		S8
Reference co-initiator		
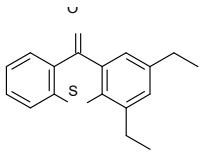		
2,4-Diethyl-9H-thioxanthen-9-one (DETX)		

3.2. Spectroscopic Characteristics of 2-Amino-4,6-Diphenyl-Pyridine-3-Carbonitrile Derivatives

3.2.1. Molecular Absorption Spectra Measurements

Absorption measurements were recorded in acetonitrile, using the SilverNova spectrometer (StellarNet, Inc., Tampa, FL, USA) in combination with a broadband tungsten-deuterium SL5 UV-Vis light source (StellarNet, Inc., Tampa, FL, USA), and a quartz cuvette with a 1.0 cm optical path. Next, the absorbance data were converted into extinction coefficients, expressed in classical units [$dm^3 \cdot mol^{-1} \cdot cm^{-1}$].

3.2.2. Fluorescence Spectra Measurements

Emission spectra measurements were carried out using the same spectrometer as with absorbance. The fluorescence characteristics of investigated compounds were measured in acetonitrile at room temperature (25 °C) using s 1.0 cm optical path quartz cells. As a light source for fluorescence measurements, a UV-LED 320 nm (UVTOP315-BL-TO39, Roithner Laser Technik GmbH, Wien, Austria) was used.

3.2.3. Steady-State Photolysis Measurements

During the measurements, cuvettes with appropriate 2-amino-4,6-diphenyl-pyridine-3-carbonitrile derivatives in acetonitrile were irradiated by:

⇒ UV-LED-365 M365L2 (from Thorlabs Inc., Newton, NJ, USA) emitting light with a wavelength at λ_{max} = 365 nm (~190 mW/cm^2, current 700 mA) over 30 min;
⇒ 405 nm M405LP1 (from Thorlabs Inc., Newton, NJ, USA) emitting light with a wavelength at λ_{max} = 405 nm (~870 mW/cm^2, current 1000 mA) over 30 min.

The photolysis of pyridine derivatives in the presence of diphenyliodonium salt ($2.7 \cdot 10^{-2}$ mol/dm^3) or ethyl 4-(dimethylamino)benzoate ($4.3 \cdot 10^{-3}$ mol/dm^3) was determined with the same parameters over 10 min. The source of light was powered by a DC2200-regulated power supply (from Thorlabs Inc., Newton, NJ, USA).

3.2.4. Fluorescence Quenching Measurements

The Quanta Master™ 40 (from Photon Technology International (PTI), currently a part of Horiba, Kioto, Japan) was used to investigate fluorescent quenching of the 2-amino-4,6-diphenyl-pyridine-3-carbonitrile derivatives in the presence of additives (i.e., diphenyliodonium salt or ethyl 4-(dimethylamino)benzoate). In the case of fluorescent quenching with iodine salt, the total amount of added quencher was about $4.023 \cdot 10^{-2}$ mol/dm^3, and in the case of fluorescent quenching with EDB, it was $8.871 \cdot 10^{-2}$ mol/dm^3.

3.3. Electrochemical Determination of Oxidation Potentials

The oxidation potentials (E_{ox} vs. Ag/AgCl) of the studied compounds were measured in an acetonitrile solution by cyclic voltammetry with tetrabutylammonium hexafluorophosphate (0.1 M) as a supporting electrolyte (Electrochemical Analyzer M161 and the Electrode Stand M164, from MTM-ANKO, Kraków, Poland). The working electrode was a platinum disk, and the reference a silver chloride electrode—Ag/AgCl. A scan rate of 0.1 V/s was used. Ferrocene was used as a standard and the potentials were determined from half peak potentials. The Gibbs free energy change ΔG_{ET} for an electron transfer between photoinitiators (diaryliodonium salt) and a co-initiator can be calculated from the classical Equation (4):

$$\Delta G_{et} = F[E_{ox}\,(D/D^{\bullet+}) - E_{red}\,(A^{\bullet-}/A)] - E_{00} - (Ze^2/\varepsilon a) \quad (4)$$

where F is the Faraday constant (F = 96485.33289(59) C mol^{-1}) and E_{ox} ($D/D^{\bullet+}$) is oxidation potential of the electron donor, E_{red} ($A^{\bullet-}/A$) is the reduction potential of the electron acceptor, E_{00} is the excited

state energy, and ($Ze^2/\varepsilon a$) is the electrostatic interaction energy for the initially formed ion pair. Parameter ($Ze^2/\varepsilon a$) is generally considered negligible in polar solvents.

The excited state energy was determined from the excitation and emission spectra using Quanta Master™ 40 spectrofluorometer (from Photon Technology International (PTI), currently a part of Horiba) at varied excitation wavelengths in the range 200–800 nm.

3.4. Molecular Orbital Calculations

The Gaussian 09 package was used for calculating the energy gap between the first triplet energy (T_1) and ground state energy (S_0). Firstly, the optimization of S_0 and T_1 states was carried out for each of the molecular structures of interest. Optimization of molecules in the ground state and first triplet excited state was performed using the density functional theory (DFT) method at a B3LYP/6-31G (d,p) level of theory. The energy gap was calculated as the difference of the total energy of the molecule in the first triplet excited state (E_{T1}) and the total energy of the molecule in the ground state (E_{S0}). The frontier molecular orbital properties were analyzed and visualized using the GaussView 5.0 software. The computations were performed on the open source PLGrid Infrastructure. PLGrid Infrastructure enables the carrying out of scientific research based on simulations and large-scale calculations using computing clusters, and also provides convenient access to distributed computing resources.

3.5. Preparation of Photocurable Compositions

The compositions for the photo-oxidative mechanism of the photopolymerization processes were prepared by dissolution of the photosensitizer and iodonium salt in a monomer in such proportions as to obtain a concentration of $3.836 \cdot 10^{-3}$ mol/dm^3 of the photosensitizer and $2.347 \cdot 10^{-2}$ mol/dm^3 (about 1% by weight) of the diphenyliodonium salt.

The compositions for the photo-reduction mechanism of the photopolymerization processes were prepared by dissolution of the photosensitizer and iodonium salt in a monomer in such proportions as to obtain the concentration of $3.836 \cdot 10^{-3}$ mol/dm^3 of the photosensitizer and $1.294 \cdot 10^{-2}$ mol/dm^3 (about 1.5% by weight) of the ethyl 4-(dimethylamino)benzoate (EDB).

The solutions were prepared in dark glass vials and were stored in the dark until needed. An excellent solubility was observed in different monomers for all biphenyl derivatives. Just prior to measurement, two drops of the composition were placed in the middle of a BaF_2 pellet (φ = 25 mm × h = 5 mm) or a polypropylene film (25 mm × 25 mm × 0.3 mm). The polypropylene film sample was covered with another polypropylene film to form a sandwich structure.

3.6. Monitoring the Photopolymerization Processes by Real-Time FTIR

The kinetics of photopolymerization were studied by two methods monitoring the course of the reaction in real time, using infrared spectroscopy with Fourier transformation (FTIR) and isothermal differential scanning calorimetry (photo-DSC). The former allowed the simultaneous determination of the conversion rate of functional groups. In turn, the technique that was used to study the kinetics of visible photopolymerization was photo-DSC.

3.6.1. Monitoring the Photopolymerization Processes by Real-Time FTIR

In order to examine the kinetics of photopolymerization by FTIR, a Nicolet iS10 (from Thermo Scientific, Waltham, MA, U.S.) spectrophotometer in transmission mode in the range 400–4000 cm^{-1}, was used. Polymerization compositions were prepared immediately prior to measurement, according to the procedure described in Section 3.5. As the decrease of absorption of the peak area was directly proportional to the number of polymerized groups, the degree of conversion of the functional group was calculated by measuring the peak area at each time of the reaction using Equation (5):

$$Conversion\ [\%] = \left(1 - \frac{A_{After}}{A_{Before}}\right) * 100\ \% \quad (5)$$

where A_{Before} is an area of the absorbance peak characteristic of the monomer used and the type of photopolymerization prior to the polymerization process, and A_{After} is an area of the same absorbance peak after the polymerization process has taken place. The values of the characteristic absorbance peak for studied monomers are given below for each type of photopolymerization.

3.6.2. Cationic Photopolymerization (CP) Measurements

The photocurable formulations (25 μm thick) were deposited on a BaF_2 pellet under air. The evolution of the epoxy group content was continuously monitored by real-time FT-IR spectroscopy at about 790 cm^{-1}. The ring-opening reaction of the cycloaliphatic epoxy group is also represented by an increasing signal of the hydroxyl groups in the region between 3100—3700 cm^{-1} and by the increasing signal of the ether groups in the band around 1080 cm^{-1}. For the vinyl monomer (TEGDVE), the photopolymerization was monitored at about 1640 cm^{-1} (C=C stretching vibration).

3.6.3. Free-radical Photopolymerization (FRP) Measurements

The experiments were carried out in laminated conditions between polypropylene films (the thickness of the composition was ~25 μm) deposited on a horizontal holder for FTIR spectrometer and were irradiated. The evolution of the double bond of acrylate TMPTA content was continuously monitored by real-time FTIR spectroscopy (Nicolet iS10, from Thermo Scientific, Waltham, MA, U.S.) at about 1634 cm^{-1} (C=C stretching vibration).

3.6.4. Thiol–Ene Photopolymerization (TEP) Measurements

The photosensitive formulations were deposited on a BaF_2 pellet under air (the thickness of the composition was ~25 μm). The evolution of the thiol (S–H) group content was continuously monitored by real-time FTIR spectroscopy at about 2570 cm^{-1} (SH stretching vibration). FTIR also monitored the double bond of methacrylate group conversion at about 1637 cm^{-1}. A weight ratio of thiol vs. ene was used in all experiments (50/50 wt. %).

3.6.5. Source of Light for Real-Time FTIR Measurements

The light sources for the real-time FTIR method were a 365 nm M365L2c UV-LED diode (~190 mW/cm^2, current 700 mA, from Thorlabs Inc. Tampa, FL, U.S.) and a 405 nm M405LP1 (~870 mW/cm^2, current 1000 mA, from Thorlabs Inc., Tampa, FL, U.S.) powered by a DC2200 regulated power supply (from Thorlabs Inc., U.S.). The UV-LED diode was initiated 10 s after the beginning of spectral registration.

3.7. Monitoring the Photopolymerization Processes by Photo Differential Scanning Calorimetry (Photo-DSC)

In order to examine the course of the photopolymerization processes using the photo-DSC method, a Netszsch DSC 204 F1 Phoenix® differential scanning calorimeter (from Netszsch-Gerätebau GmbH, Selb, Germany) adapted for photochemical measurements was used. Photosensitive compositions (prepared immediately before the measurement according to the procedure described in Section 3.5), were weighed on a micro-scale in amounts of 2 mg (+/−0.005 mg) into aluminum DSC crucibles (from Netszsch-Gerätebau GmbH, Selb, Germany). The crucible, together with the test sample, was placed in the chamber of the photo-DSC apparatus. The chamber was washed with an inert gas (nitrogen with purity = 99.999%) at a flow rate of 40 mL/min throughout the measurement period. Then, the visible LED lamp emitting light with λ_{max} = 405 nm and intensity of 1 mW/cm^2 (+/−0.09 mW/cm^2) was turned on (the radiation intensity was measured using an OmniCure R2000 radiometer (from Excelitas Technologies®, Mississagua, ON, Canada) and the sample was irradiated by opening the diaphragm covering the measuring chamber. As a reference, an empty DSC crucible identical to the one in which the test sample was located was used. The measurement took place in a nitrogen atmosphere and continued until a steady stream of heat was established. All measurements were conducted at isothermal conditions of 25 °C. The obtained measurement data were directly processed by the Netszsch Proteus® software (from

Netszsch-Gerätebau GmbH, Selb, Germany) and saved as ASCII text files. They contained temperature, heat flow, and polymerization rates. For the calculations, it was assumed that the heat of photopolymerization for acrylates and epoxides was 86 kJ/mol and 94 kJ/mol [42] respectively.

Source of Light for Photo-DSC Measurements

A narrow band 405 nm visible LED Bluepoint eco light source (from Dr. Hönle AG, Gräfelfing, Germany) was used for investigating the initiating system properties at conditions known from modern 3D printers equipped with 405 nm LEDs or 405 nm laser diodes. The illumination power of the visible Bluepoint LED eco light source was 25 mW/cm^2 measured by the OmniCure R2000 radiometer for maximal similarity with conditions observed at common DLP printers.

The broad band source of light used in the experiments was a 200 W medium pressure mercury lamp (MPM) OmniCure S2000 (from Excelitas Technologies®, Ontario, Canada) calibrated for 75 mW/cm^2 illumination power by the OmniCure R2000 radiometer. The MPM lamp was used with a dedicated bandpass filter of 400–500 nm to provide conditions known in 3D printers equipped with different light sources.

3.8. 3D Printing Equipment with Different Visible Light Sources

In order to examine the properties of the obtained formulations directly into the additive manufacturing process, three different ways of 3D printing were chosen.

3.8.1. The Laser Engraver Printer Machine

Firstly, compositions were poured into a 20 × 30 × 2 mm polylactide (PLA) vat with a glass bottom, and irradiated by a 405 nm 500 mW diode laser at a distance of 7 cm (spot diameter, ~75 μm) using the Laser Engraver Printer machine (NEJE DK-8-KZ, NEJE DK-8-KZ, from Shenzhen Zhixinjie Technologym Shenzen, Guangdong, China). This plotter works periodically, illuminating tiny spots on the surface of the photopolymerization vat for a certain amount of time (10–100 ms) without direct adjustment of the laser power. Following this test, the liquid resin was removed and the prints were washed with isopropyl alcohol. After drying, without any post-curing operation, parameters such as the resolution of the obtained prints were compared at room temperature.

3.8.2. SLA Home-Made 3D Printer

The second experiment involved the printing of a multilayer combination on a home-made 3D printer consisting of a CNC machine equipped with a 1500 mW 405 nm diode laser (NEJE PWM Laser Module, from Shenzhen Zhixinjie Technologym Shenzen, Guangdong, China) (Figure 22). This equipment stands out, as it has a constant laser beam and adjustable laser power. These are advantages affording better control of the amount of light applied to the cured formulation.

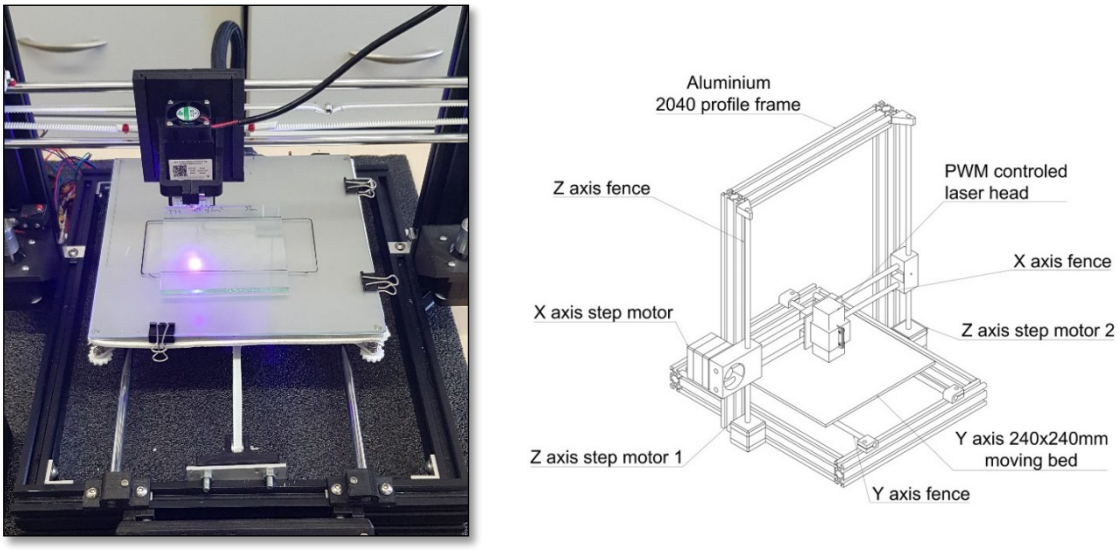

Figure 22. Home-made Computerized Numerical Control (CNC) machine with a 405 nm laser diode with continuous beam and fully adjustable laser power (constructed by P.Fiedor).

3.9. Microscope Images

The generated 3D objects were observed under an optical stereo microscope (BRESSER Advance ICD 10–160x Zoom Stereo-Microscope, Bresser GmbH, Rhede, Germany).

4. Conclusions

In the present paper, 2-amino-4,6-diphenyl-pyridine-3-carbonitriles derivatives were proposed as an interesting scaffold for the development of new high-performance photoinitiators upon near-UV or visible LEDs for the photoinitiation of both cationic polymerization of epoxides and vinyl monomers, as well as the free-radical polymerization of acrylates and thiol–ene photopolymerization of methacrylates and thiol monomers. These novel photosensitizers in combination with different types of additives, e.g., iodonium salt or in the presence of amine as a co-initiator, can act as a bimolecular photoinitiating system via the photo-reduction or photo-oxidation pathways respectively. Moreover, it was shown that the best properties of photosensitizers are exhibited by 2-amino-4-(4-methylthiophenyl),6-phenyl pyridine-3-carbonitrile (S4), 2-amino-4-phenyl-6-(4-methylthiophenyl)pyridine-3-carbonitrile (S5), 2-amino-4,6-bis(4-methylthiophenyl)--pyridine-3-carbonitrile (S6), 2-amino-4-(4-methylthiophenyl)-6-(4-methoxyphenyl)-pyridine-3-carbonitrile (S7), and 2-amino-4-(4-methoxyphenyl)-6-(4-methylthiophenyl)-pyridine-3-carbonitrile (S8). Considering processability and stability in the printing process, the 2-amino-4,6-diphenyl-pyridine-3-carbonitrile derivatives in combination with diphenyliodonium salt seemed to be good candidates for visible photoinitiating systems for 3D printing, in particular for a photosensitive purely cationic formulation based on cycloaliphatic epoxide and vinyl monomers. Overall, Compounds S4, S5, S6, S7, and S8 exhibited the best properties during 3D printing at the proposed parameters. Other studied compounds required more illumination power and/or slower laser head passing. Moreover, for the presented SLA 3D printing processes, the 2-amino-4,6-diphenyl-pyridine-3-carbonitrile derivatives can not only be used as visible photosensitizers for iodonium salt but also act as absorbing agents for controlling curing depth, especially in multilayer 3D photopolymerization printing processes.

Supplementary Materials: The following are available online at www.mdpi.com/xxx/s1. The section about the synthesis of 2-amino-4,6-diphenylpyridine-3-carbonitrile derivatives and spectroscopic characterization; Figures S1–S9: ^{1}H NMR spectra of synthesized 2-amino-4,6-diphenylpyridine-3-carbonitrile derivatives; Figures S10–S16: ^{13}C NMR spectra of synthesized 2-amino-4,6-diphenylpyridine-3-carbonitrile derivatives; Figures S17–S32: cyclic voltammetry curves showing oxidation and reduction processes of

2-amino-4,6-diphenylpyridine-3-carbonitrile derivatives in acetonitrile; Figures S33–S40: absorption and fluorescence spectra for the determination of the excited singlet state energy for investigated of 2-amino-4,6-diphenylpyridine-3-carbonitrile derivatives in acetonitrile. The section about the optimized structures and HOMO and LUMO orbitals of investigated 2-amino-4,6-diphenylpyridine-3-carbonitrile derivatives free molecules determined with the use of uB3LYP/6-31G* level of theory; Figures S41–S56: fluorescence quenching with diphenyliodonium hexafluorophosphate of investigated 2-amino-4,6-diphenylpyridine-3-carbonitrile derivatives together with Stern-Volmer correlation; Figures S57–S72: fluorescence quenching with EDB of investigated 2-amino-4,6-diphenylpyridine-3-carbonitrile derivatives together with Stern-Volmer correlation; Figures S73–S88: steady state photolysis upon exposure with UV-LED at 365 nm for of investigated 2-amino-4,6-diphenylpyridine-3-carbonitrile derivatives in acetonitrile; Figures S89–104: steady state photolysis upon exposure with LED at 405 nm for of investigated 2-amino-4,6-diphenylpyridine-3-carbonitrile derivatives in acetonitrile; Figures S105–112: steady state photolysis upon exposure with LED @405 nm for of investigated 2-amino-4,6-diphenylpyridine-3-carbonitrile derivatives and EDB in acetonitrile.

Author Contributions: J.O. conceived the project, designed the research, designed the new photosensitizers, contributed to all aspects of the study, analyzed the whole data sets, and wrote final version of the paper. P.F. performed the all photopolymerization experiments (including 3D printing experiments and the construction of the home-made SLA 3D printer), and assisted in writing and editing the manuscript. Moreover, P.F. and P.S. performed the photophysical characterizations of the new photosensitizers. A.C.-B., P.F., and M.G. performed the synthesis of the different 2-amino-4,6-diphenyl-pyridine-3-carbonitriles derivatives reported in this work and characterized the chemical structures of these photosensitizers by the usual techniques. M.P. performed the electrochemistry research and molecular orbital calculations. All authors have read and agreed to the final version of the manuscript.

Funding: This research was funded by the Foundation for Polish Science (Warsaw, Poland), TEAM TECH project Grant No. TEAM TECH/2016-2/15 (POIR.04.04.00-00-204B/16-00), "Molecular design, synthesis and application of photoinitiator-catalysts (PICs) for photopolymerization reactions." The authors are grateful to the Foundation for Polish Science (Warsaw, Poland) REINTEGRATION/2016-1/4 (POIR.04.04.00-00-1E42/16-00) for financing part of the synthetic research. Moreover, PhD student P.F. is grateful for the support received in the form of a scholarship by a Synthos Generation Training Program co-financed by Synthos S.A. (Oświęcim, Poland). The computations were performed on open source software by PLGrid Infrastructure.

Conflicts of Interest: The authors declare no conflicts of interest.

References

1. Ligon, S.C.; Liska, R.; Stampfl, J.; Gurr, M.; Mülhaupt, R. Polymers for 3D Printing and Customized Additive Manufacturing. *Chem. Rev.* **2017**, *117*, 10212–10290.
2. Vaezi, M.; Seitz, H.; Yang, S.F. A Review on 3D Micro-Additive Manufacturing Technologies. *Int. J. Adv. Manuf. Technol.* **2013**, *67*, 1721–1754.
3. Layani, M.; Wang, X.; Magdassi, S. Novel Materials for 3D Printing by Photopolymerization. *Adv. Mater.* **2018**, *30*, 1706344.
4. Hossam, K.; Soham, W.; Changxue, X.; Fakhrul, A. Digital light processing (DLP) 3D-printing technology and photoreactive polymers in fabrication of modified-release tablets. *Eur. J. Pharm. Sci.* **2019**, *135*, 60–67.
5. Tumbleston, J.R.; Shirvanyants, D.; Ermoshkin, N.; Janusziewicz, R.; Johnson, A.R.; Kelly, D.; Chen, K.; Pinschmidt, R.; Rolland, J.P.; Ermoshkin, A.; et al. Continuous Liquid Interface of 3D Objects. *Science* **2015**, *347*, 1349–1352.
6. Dilag, J.; Chen, T.; Li, S.; Bateman, S.A. Design and direct additive manufacturing of three-dimensional surface micro-structures using material jetting technologies. *Addit. Manuf.* **2019**, *27*, 167–174.
7. Kerekes, T.W.; Lim, H.; Joe, W.Y.; Yun, H.J. Characterization of process–deformation/damage property relationship of fused deposition modeling (FDM) 3D-printed specimens. *Addit. Manuf.* **2019**, *25*, 532–544.
8. Shahrubudin, N.; Lee, T.C.; Ramlan, R. An Overview on 3D Printing Technology: Technological, Materials, and Applications. *Procedia Manuf.* **2019**, *35*, 1286–1296.
9. Bandyopadhyay, A.; Bose, S. *Additive Manufacturing*, 1st ed.; CRC Press: Boca Raton, FL, USA, 2015.
10. Bagheri, A.; Jin, J. Photopolymerization in 3D Printing. *ACS Appl. Polym. Mater.* **2019**, *1*, 593–611.
11. Zhang, J.; Xiao, P. 3D Printing of Photopolymers. *Polym. Chem.* **2018**, *9*, 1530–1540.
12. Ortyl, J. Cationic Photoinitiators. In *Photopolymerisation Initiating Systems*, 1st ed.; Lalevée, J., Fouassier, J.P., Eds.; Royal Society of Chemistry: Croydon, UK, 2018; pp. 74–130.

13. Ortyl, J.; Popielarz, R. New photoinitiators for cationic polymerization. *Polimery* **2012**, *57*, 7–8.
14. Dietlin, C.; Schweizer, S.; Xiao, P.; Zhang, J.; Morlet-Savary, F.; Graff, B.; Fouassier, J.P.; Lalevée, J. Photopolymerization upon LEDs: New photoinitiating systems and strategies. *Polym. Chem.* **2015**, *6*, 3895–3912.
15. Hola, M.; Pilch, M.; Galek, M.; Ortyl, J. New versatile bimolecular photoinitiating systems based on amino-m-terphenyl derivatives for cationic, free-radical and thiol-ene photopolymerization under low intensity UV-A and visible light sources. *Polym. Chem.* **2020**, *11*, 480–495.
16. Ortyl, J.; Milart, P.; Popielarz, R. Applicability of aminophthalimide probes for monitoring and acceleration of cationic photopolymerization of epoxides. *Polym. Test.* **2013**, *32*, 708–715.
17. Kostrzewska, K.; Ortyl, J.; Dobosz, R.; Kabatc, J. Squarylium dye and onium salts as highly sensitive photoradical generators for blue light. *Polym. Chem.* **2017**, *22*, 3464–3474.
18. Kabatc, J.; Ortyl, J.; Kostrzewska, K. New kinetic and mechanistic aspects of photosensitization of iodonium salts in photopolymerization of acrylates. *RCV Adv.* **2017**, *66*, 41619–41629.
19. Tomal, W.; Pilch, M.; Chachaj-Brekiesz, A.; Ortyl, J. Development of new high-performance biphenyl and terphenyl derivatives as versatile photoredox photoinitiating systems and their applications in 3D printing photopolymerization processes. *Catalysts* **2019**, *9*, 827.
20. Ortyl, J.; Wilamowski, J.; Milart, P.; Galek, M.; Popielarz, R. Relative sensitization efficiency of fluorescent probes/sensitizers for monitoring and acceleration of cationic photopolymerization of monomers. *Polym. Test.* **2015**, *48*, 151–159.
21. Ortyl, J.; Popielarz, R. The performance of 7-hydroxycoumarin-3-carbonitrile and 7-hydroxycoumarin-3-carboxylic acid as fluorescent probes for monitoring of cationic photopolymerization processes by FPT. *J. Appl. Polym. Sci.* **2013**, *128*, 1974–1978.
22. Kamińska, I.; Ortyl, J.; Popielarz, R. Applicability of quinolizino-coumarins for monitoring free radical photopolymerization by fluorescence spectroscopy. *Polym. Test.* **2015**, *42*, 99–107.
23. Ortyl, J.; Sawicz-Kryniger, K.; Galek, M.; Popielarz, R. Monitoring of cationic photopolymerization with stilbene derivatives as fluorescent probes. *Przem. Chem.* **2010**, *89*, 1642–1646.
24. Kamińska, I.; Ortyl, J.; Popielarz, R. Mechanism of interaction of coumarin-based fluorescent molecular probes with polymerizing medium during free radical polymerization of a monomer. *Polym. Test.* **2016**, *55*, 310–317.
25. Ortyl, J.; Galica, M.; Popielarz, R.; Bogdał, D. Application of a carbazole derivative as a spectroscopic fluorescent probe for real time monitoring of cationic photopolymerization. *Pol. J. Chem. Technol.* **2014**, *16*, 75–80.
26. Hola, E.; Ortyl, J.; Jankowska, M.; Pilch, M.; Galek, M.; Morlet-Savary, F.; Graff, B.; Dietlinc, C.; Lalevée, J. New bimolecular photoinitiating systems based on terphenyl derivatives as highly efficient photosensitizers for 3D printing application. *Polym. Chem.* **2020**, doi:10.1039/C9PY01551E.
27. Lapim, S.C.; Snyder, J.R.; Sitzmann, E.V.; Barnes, D.K.; Green, G.D. Stereolithography Using Vinyl Ether-Epoxide Polymers. U.S. Patent 5,437,964, 1 August 1995.
28. Lapim, S.C.; Brautigam, R.J. Stereolithography Using Vinyl Ether Based Polymers. U.S. Patent 5,506,087, 9 April 1996.
29. Al Mousawi, A.; Dumur, F.; Garra, P.; Toufaily, J.; Hamieh, T.; Goubard, F.; Bui, T.-T.; Graff, B.; Gigmes, D.; Fouassier, J.-P.; et al. Azahelicenes as visible light photoinitiators for cationic and radical polymerization: Preparation of photoluminescent polymers and use in high performance LED projector 3D printing resins. *J. Polym. Sci. A Polym. Chem.* **2017**, *55*, 1189–1199.
30. Ortyl, J.; Fiedor, P.; Chachaj-Brekiesz, A.; Pilch, M.; Hola, E.; Galek, M. The Applicability of 2-amino-4, 6-diphenyl-pyridine-3-carbonitrile Sensors for Monitoring Different Types of Photopolymerization Processes and Acceleration of Cationic and Free-Radical Photopolymerization Under Near UV Light. *Sensors* **2019**, *19*, 1668.
31. Crivello, J.V. Cationic Polymerization—Iodonium and Sulfonium Salt Photoinitiators. *Adv. Polym. Sci.* **1984**, *62*, 1–44.
32. Rehm, D.; Weller, A.H. Kinetics of fluorescence quenching by electron and H-atom transfer. *Isr. J. Chem.* **1970**, *8*, 259–271.
33. Romańczyk, P.P.; Kurek, S.S. The Reduction Potential of Diphenyliodonium Polymerisation Photoinitiator Is Not −0.2 V vs. SCE. A Computational Study. *Electrochim. Acta.* **2017**, *225*, 482–485.

34. Strehmel, B.; Ernst, S.; Reiner, K.L.; Keil, D.; Lindauer, H.; Baumann, H. Application of NIR-photopolymers in the graphic industry: From physical chemistry to lithographic applications. *Z. Phys. Chem.* **2014**, *228*, 129–153.
35. Fouassier, J.-P.; Lalevee, J. *Photoinitiators for Polymer Synthesis: Scope, Reactivity and Efficiency*; Wiley-VCH Verlag: Weinheim, Germany, 2012.
36. Hoyle, C.E.; Bowman, C.N. Thiol–Ene Click Chemistry. *Angew. Chem. Int. Ed.* **2010**, *49*, 1540–1573.
37. Chen, L.; Wu, Q.; Wei, G.; Liu, R.; Li, Z. Highly stable thiol-ene systems: From their structure—Property relationship to DLP 3D printing. *J. Mater. Chem. C* **2018**, *6*, 11561–11568.
38. Sycks, D.G.; Wu, T.; Park, H.S.; Gall, K. Tough, Stable Spiroacetal Thiol-Ene Resin for 3D Printing. *J. Appl. Polym. Sci.* **2018**, *135*, 46259.
39. Oesterreicher, A.; Wiener, J.; Roth, M.; Moser, A.; Gmeiner, R.; Edler, M.; Pinter, G.; Griesser, T. Tough and Degradable Photopolymers Derived from Alkyne Monomers for 3D Printing of Biomedical Materials. *Polym. Chem.* **2016**, *7*, 5169–5180.
40. Marx, P.; Romano, A.; Roppolo, I.; Chemelli, A.; Mühlbacher, I.; Kern, W.; Chaudhary, S.; Andritsch, T.; Sangermano, M.; Wiesbrock, F. 3D-Printing of High-κ Thiol-Ene Resins with Spiro-Orthoesters as Anti-Shrinkage Additive. *Macromol. Mater. Eng.* **2019**, *304*, 1900515.
41. Andrzejewska, E.; Zych-Tomkowiak, D.; Andrzejewski, M.; Hug, G.L.; Marciniak, B. Heteroaromatic Thiols as Co-initiators for Type II Photoinitiating Systems Based on Camphorquinone and Isopropylthioxanthone. *Macromolecules* **2006**, *39*, 3777–3785.
42. Roberts, D.E. Heats of Polymerization. A Summary of Published Values and Their Relation to Structure, Research Paper RP20073. *J. Res. Natl. Bur. Stand.* **1950**, *44*, 221–232.